

# Origin and provenance of Lower Jurassic clastic rocks in the Badaowan Formation, Dachanggou Basin, Northern Xinjiang, China: Constraints on Early Jurassic weathering and depositional processes

Xingxuan Lei<sup>a,b</sup>, Pingchang Sun<sup>a,b,c,\*</sup>, Junxian Wang<sup>d,e</sup>, Hongliang Dang<sup>a,f,g</sup>, Xuemei Tian<sup>h</sup>, Zhisheng Luan<sup>i</sup>, Zhuo Wang<sup>j</sup>

<sup>a</sup> College of Earth Sciences, Jilin University, Changchun 130061, China

<sup>b</sup> Key Laboratory of Oil Shale and Symbiotic Energy Minerals, Changchun 130061, Jilin Province, China

<sup>c</sup> State Key Laboratory of Deep Earth Exploration and Imaging, Changchun 130061, Jilin Province, China

<sup>d</sup> Beijing Research Institute of Uranium Geology, Beijing 100029, China

<sup>e</sup> National Key Laboratory of Uranium Resource Exploration-Mining and Nuclear Remote Sensing, Beijing 100029, China

<sup>f</sup> Technology Innovation Center for Exploration and Exploitation of Strategic Mineral Resources in Plateau Desert Region, Ministry of Natural Resources, Xining 810000, China

<sup>g</sup> Qinghai Geological Survey, Xining 810000, China

<sup>h</sup> Changchun Medical College, Changchun 130031, China

<sup>i</sup> Liaohu Oilfield Company, PetroChina, Panjin, Liaoning 124010, China

<sup>j</sup> Oil and Gas Technology Research Institute, PetroChina Changqing Oilfield Company, Xi'an, Shanxi 710018, China

## ARTICLE INFO

Editor: Howard Falcon-Lang

### Keywords:

Provenance analysis  
Detrital zircon  
East Junggar  
Early Jurassic

## ABSTRACT

The Dachanggou Basin, a small intermontane basin in the southern Central Asian Orogenic Belt (CAOB), preserves high-resolution Early Jurassic clastic records of regional tectonics, orogenic uplift, and paleoclimatic changes. We integrate petrological, geochemical, and detrital zircon U-Pb data from the Badaowan Formation. Geochemical signatures demonstrate minimal alteration by sedimentary recycling, hydraulic sorting, or diagenesis. High Chemical Index of Alteration (CIA) values and sandstone petrography indicate moderate to strong chemical weathering. Geochemical data indicate that the Badaowan Formation was deposited in a post-collisional intracontinental rift basin, with mudstone (including oil shale) detritus primarily sourced from a felsic volcanic arc within a stable continental island arc setting. Sandstone petrology, dominated by felsic volcanic lithics and quartz, supports this interpretation. Detrital zircon ages reveal three dominant populations and minor Proterozoic groups, recording multiple magmatic episodes with limited ancient recycling. The 530–480 Ma zircons derive from Cambrian arcs north of East Junggar and Permian Bogda Mountain sediments. The 430–390 Ma and 360–270 Ma groups correlate with magmatism in the Yemaquan and Bogda arcs. The youngest zircon at 250 Ma suggests that Indosinian orogenesis in East Junggar began no earlier than this time. Provenance shifted from proximal Yemaquan Arc to distal Bogda Arc during the Early Jurassic, coinciding with increasingly warmer, more humid climatic conditions. This transition implies tectonic uplift and erosional exhumation of the eastern Bogda Orogenic Belt (BOB) by the late deposition stage of the Badaowan Formation.

## 1. Introduction

Sediment provenance analysis is a key part of basin analysis and plays a vital role in reconstructing paleoenvironments and paleoclimates, tracing source region tectonics, and studying basin coupling (Dickinson and Gehrels, 2009; Xu et al., 2017; Qiu et al., 2022). The geochemical composition of clastic rocks is controlled by source rock

lithology, weathering intensity, and tectonic activity (Nesbitt and Young, 1982; Taylor and McLennan, 1985; Condie, 1993). Consequently, geochemical data has been extensively utilized to identify sediment sources and lithology (Li et al., 2019; Rahim and Li, 2025), assess the chemical weathering history (Fu et al., 2023; Awan et al., 2025a), and investigate tectonic settings (Bhatia and Crook, 1986; Roser and Korsch, 1986, 1988). Studies (Pearce, 1983; Bhatia, 1985; Taylor

\* Corresponding author at: College of Earth Sciences, Jilin University, Jianshe Street 2199, Changchun 130061, China.

E-mail address: [sunpingchang711@126.com](mailto:sunpingchang711@126.com) (P. Sun).

and McLennan, 1985; Cox et al., 1995) have demonstrated that immobile trace elements such as La, Th, Ti, Zr, Sc, Co, and rare earth elements (REE) remain stable during geological processes (Holail and Moghazi, 1998), making them effective indicators for deciphering source rock composition and tectonic setting (Condie, 1991, 1993; Cullers, 1994; Li et al., 2025a, 2025b). Furthermore, major elements like Na, Ca, K, Al, and Ti exhibit variable mobility due to chemical differences, and thus

serve as reliable proxies for paleoclimate and chemical weathering reconstructions (Perri, 2020). However, because sedimentary rock geochemistry reflects multiple overlapping factors, the preserved geological information can be complex. Integrating petrological, geochemical, and detrital zircon data has proven effective for clarifying sediment source characteristics and tectonic settings (Geslin et al., 1999; Mu et al., 2024).

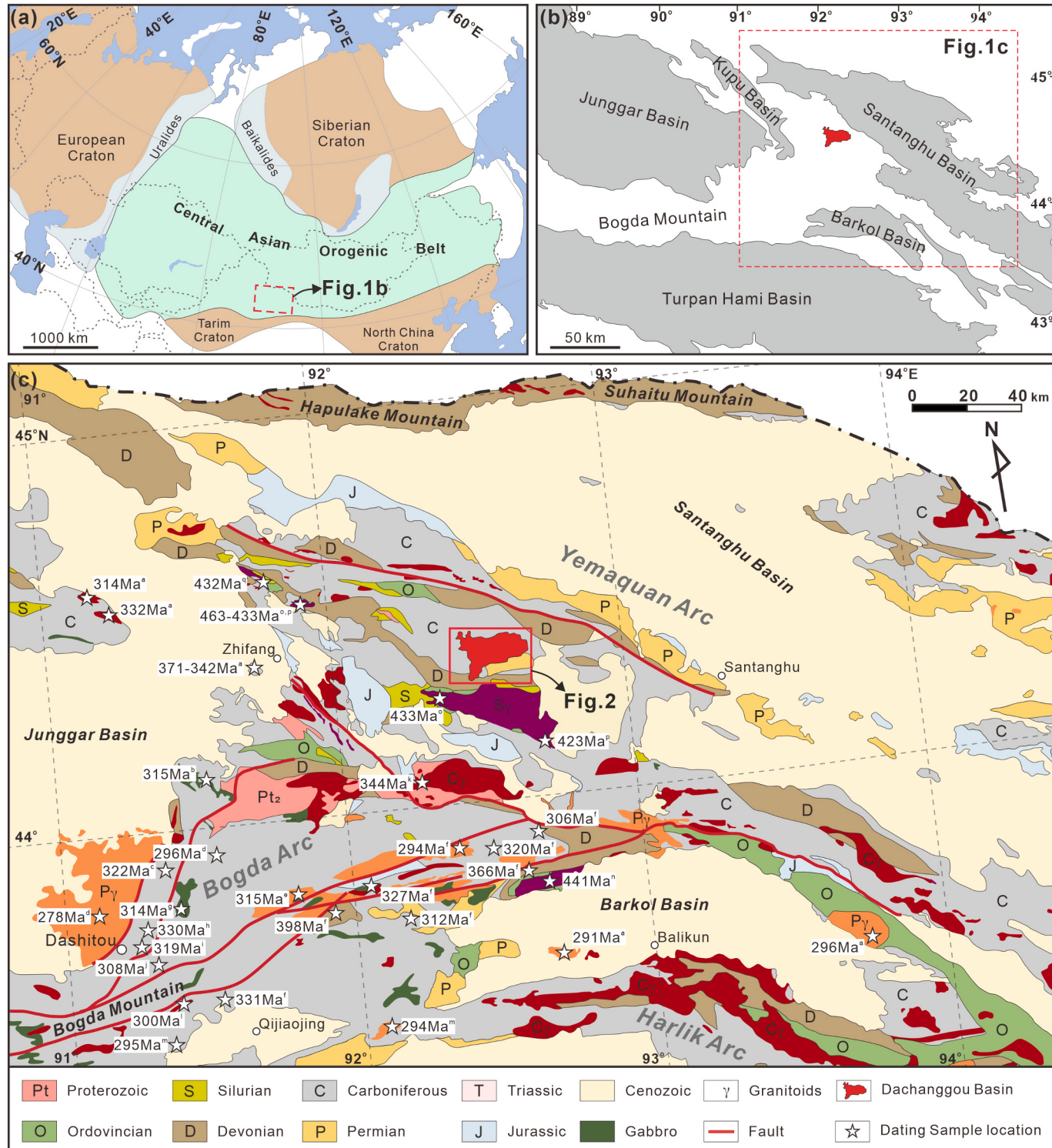


**Fig. 1.** (a) Tectonic outline of the Central Asian Orogenic Belt (modified after Jahn et al., 2000). (b) Tectonic units map of Northwest China, showing the location of the Dachanggou Basin (modified after Dong et al., 2010). (c) Simplified geological map of the East Junggar (modified after Li et al., 2013; Wang et al., 2020), displaying age data of magmatic rocks (see Table S1 for detailed information).

The Dachanggou Basin is a coal- and oil shale-bearing Jurassic intermontane basin in northwestern China, located structurally between the Junggar, Santanghu, and Barkol basins (Fig. 1b). Unlike larger inherited basins such as the Junggar, Santanghu, and Turpan-Hami basins that formed from the Carboniferous to the Jurassic (Ji et al., 2018), this basin's limited tectonic setting makes it highly responsive to sediment supply, source weathering, and environmental changes. Previous studies on the Badaowan Formation mainly focused on paleontology, paleoclimatology, and source rock evaluation (Wang et al., 2021, 2022; Bai et al., 2023). However, the provenance, weathering history, and their relationship to regional tectonic evolution in this basin remain poorly understood. We investigate the lithofacies and geochemical attributes of clastic rocks from the Lower Jurassic Badaowan Formation, integrating detrital zircon U-Pb data through multi-proxy analysis to reconstruct paleoweathering intensity, source rock composition, and tectonic settings. This study provides insights into the tectonic evolution of the southern CAOB and enhances understanding of source-to-sink systems in NW China.

## 2. Geological setting

The Dachanggou Basin is located in northern Xinjiang Uygur Autonomous Region, China. It belongs to the Tengbala-Karamaili Paleozoic composite trench-arc belt within the Junggar Microplate of the Kazakhstan Plate in the southern part of the CAOB (Dong et al., 2010) (Fig. 1a). The basin lies among several Mesozoic sedimentary basins, including the Junggar, Santanghu, Turpan-Hami, and Barkol basins (Carroll, 1998; Deng et al., 2017) (Fig. 1b). Since the Mesozoic, these basins have undergone similar tectonic histories and developed comparable stratigraphic frameworks (Carroll, 1998; Tao et al., 2017). Under similar regional paleoclimatic conditions, the Early Jurassic period was marked by widespread subsidence, leading to the deposition of thick lacustrine dark mudstone sequences across these basins (Deng et al., 2010; Xiao and Santosh, 2014).

The regional tectonic history provides a key framework for sediment provenance analysis and interpretation of tectonic settings. Tectonic-magmatic activities in northern Xinjiang were primarily controlled by the southward assembly of multiple tectonic units (microcontinental blocks) and the multi-stage evolution of the Paleo-Asian Ocean (PAO) (Windley et al., 2007; Xiao et al., 2008, 2010; Ren et al., 2014). From the Late Ordovician to the Silurian, the Armantai Ocean (a PAO branch) in northern Junggar began to subduct northward beneath the Altai island arc (Wong et al., 2010; Long et al., 2012; An et al., 2021), forming an accretionary complex along its southern margin (Xiao et al., 2009). Concurrently, the Kalamaili Ocean to the south initiated northward subduction beneath East Junggar (Li et al., 2009; Zhang et al., 2013b; Zhang et al., 2015), leading to the formation of oceanic island arc assemblages, including basaltic and dioritic rocks from the Dulate Arc (458–422 Ma, Luo et al., 2017), and andesitic, granitic, and dioritic suites from the Yemaquan Arc (466–422 Ma; Xiao et al., 2013; Huang et al., 2013; Zhang et al., 2013b; Guo et al., 2013; Xu et al., 2020). The continuous subduction of the Kalamaili Ocean formed the main body of the Yemaquan and Dulate arcs from the Late Silurian to Middle Devonian (Xiao et al., 2009). This period marks the onset of North Tianshan Ocean subduction, which generated the Bogda Arc during the Late Devonian to Early Carboniferous (Shu et al., 1999, 2000; Charvet and Shu, 2007; Charvet et al., 2011) (Fig. 1c). The PAO closed in northern Xinjiang before the Early Carboniferous (Xiao et al., 2004; Windley et al., 2007; Zhang et al., 2013b; Zhang et al., 2015; Li et al., 2020), with large-scale collision-related granitic activity persisting until the end of the Permian (Laurent-Charvet et al., 2002; Chen and Jahn, 2004; Wang and Xu, 2006; Yang et al., 2011; Luo et al., 2017; Li et al., 2020; Wang et al., 2023b; Zhao et al., 2024). The Indosinian Orogeny (Early Triassic) initiated an intracontinental extensional tectonic regime (Yang et al., 2015), and the Qiangtang–Eurasia Block collision (Late Triassic) marked western China's full transition into this extensional setting (Hendrix

et al., 1992; Deng et al., 2017; Tao et al., 2017), under which the Dachanggou Basin underwent major sedimentation.

The Dachanggou Basin is 11 km wide from north to south and 23 km long from east to west, with a total area of approximately 240 km<sup>2</sup> (Fig. 2a). The late Indosinian Orogeny (Late Permian) induced crustal uplift and widespread erosion in the East Junggar (Xiao and Santosh, 2014; Xu et al., 2014; Liu et al., 2018), leading to the regional absence of Triassic strata (Fig. 1c). Basin subsidence began in the early Early Jurassic, initiating the deposition of coarse-grained clastic rocks such as conglomerates and conglomeratic sandstones, mainly formed in fluvial and alluvial fan environments, which constitute the first member of the Badaowan Formation (J<sub>1</sub>b<sup>1</sup>). As subsidence continued and the climate became warmer and more humid, sedimentation gradually shifted to fine-grained deposits, including fine sandstones, siltstones, and mudstones, along with oil shale and coal seams, forming the second member of the Badaowan Formation (J<sub>1</sub>b<sup>2</sup>) (Zhou et al., 2010; Zhang et al., 2018) (Fig. 2c). During the Late Jurassic, the Yanshanian Orogeny triggered northward movement and collision of the Lhasa Block with the Qiangtang Block, leading to crustal uplift and intense erosion and the absence of Middle–Late Jurassic strata (Yang et al., 2015; Deng et al., 2017). The Sangonghe Formation unconformably overlies the Badaowan Formation and is itself overlain by the Lower Cretaceous Qingshuihe Formation (Fig. 2b). Late-stage differential uplift and erosion shaped the basin, with its boundaries primarily defined by northwest erosion and eastern sedimentation (Wang et al., 2021; Fig. 2a).

## 3. Sampling and analytical methods

### 3.1. Sampling

All samples were collected from well ZK1601 (44°22'1.9"N, 92°28'21.4"E), located near the open-pit mining area of the Shitanyao oil shale mine in northwestern Barkol County (Fig. 2a). This borehole primarily exposes fine-grained sediments from the Lower Jurassic Badaowan Formation, which hosts oil shale-bearing strata. A total of twenty-eight medium- to fine-grained sandstone samples were selected for framework petrography, fourteen mudstone samples (including silty mudstones) and seventeen oil shale samples were used for the whole-rock geochemical analyses. In addition, two fine-grained sandstone samples (19XJ-1 and 19XJ-2), each weighing approximately 6 kg, were collected for detrital zircon separation and U-Pb dating. The sampling depths for each type of analysis are summarized in Fig. 2c.

### 3.2. Framework petrography

Thin sections were prepared from the sandstone samples, and their petrographic characteristics, including mineral composition, grain size, sorting, and rounding, were examined under a polarizing microscope and systematically recorded. For each thin section, three hundred (300) points were analyzed using the Gazzi-Dickinson method (Dickinson, 1985). Medium- to coarse-grained detrital grains were selected for point counting to reduce potential biases caused by grain-size effects (Ingersoll et al., 1984).

### 3.3. Whole-rock geochemistry

Whole-rock geochemical analyses were conducted at the Beijing Research Institute of Uranium Geology, Beijing, China. The samples were cleaned and their surfaces removed to avoid contamination, followed by crushing into powders with a particle size finer than 200 mesh (diameter < 0.075 mm) using a tungsten carbide steel pot. Major elements were analyzed using Inductively Coupled Plasma Optical Emission Spectrometer (ICP-OES), while trace elements and rare earth elements (REE) were determined by Agilent 7500a Laser Ablation Inductively Coupled Plasma Mass Spectrometer (LA-ICP-MS). The US Geological Survey standard sample AGV2 and international standard

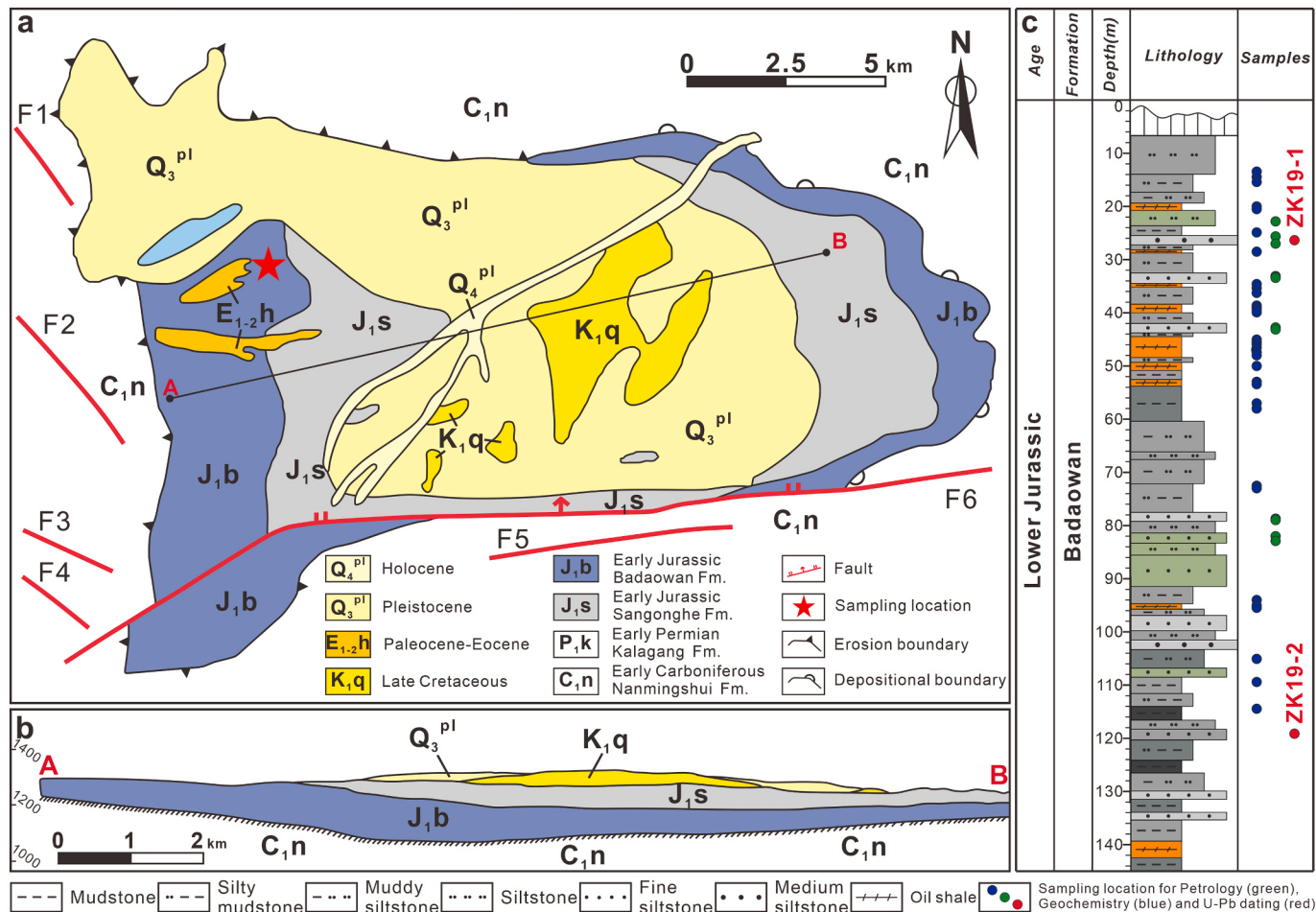


**Fig. 2.** (a) Geological map of the Dachanggou Basin with the sampling location indicated. (b) Structural profiles of the Dachanggou Basin illustrating the basin architecture (Wang et al., 2022). (c) Lithologic column of the sampling well.

samples GSR-1 (granite) and GSR-3 (basalt) were used for monitoring and analyzing accuracy and precision (Govindaraju, 1994). Loss on ignition (LOI) was determined by heating the sample at 1000 °C for 1 h. Analytical precision was better than 2 % for all major oxides and less than 5 % for trace elements.

#### 3.4. Detrital zircon U-Pb dating

Samples were crushed to 60 mesh powder, and zircon grains (200 pieces per sample) were separated using heavy liquid and magnetic techniques, followed by purification through handpicking under a binocular microscope. Representative zircon grains were selected manually, mounted in epoxy resin discs, polished, and coated with gold. Cathodoluminescence (CL) imaging was employed to examine the internal structures of zircons and to identify optimal sites for U-Pb dating. The LA-ICP-MS U-Pb dating was conducted using an Agilent 7900 ICP-MS instrument (United States) coupled with a GeoLasPro 193 nm ArF excimer laser system (Germany), following the methodology of Zong et al. (2017). Detailed instrumental operating conditions and data reduction methodologies have been described by Liu et al. (2010). Standard zircon 91500 ( $^{206}\text{Pb}/^{238}\text{U}$  age =  $1062.4 \pm 0.2$  Ma; Wiedenbeck et al., 1995) and Plesovice zircon were used as external standards and monitoring samples, respectively. Time-drift correction and quantitative calibration for trace-element analyses and U-Pb dating were performed using ICP MS Data Cal 10.0 (Liu et al., 2010). After applying common Pb correction based on the method of Andersen (2002), the Isoplot 3.0 software (Ludwig, 2003) was used to generate the age concord plot and probability density plot. We report  $^{206}\text{Pb}/^{238}\text{U}$  ages for zircon grains

younger than 1000 Ma and  $^{206}\text{Pb}/^{207}\text{Pb}$  ages for grains older than 1000 Ma.

## 4. Results

### 4.1. Sandstone petrography

Detrital grains from sandstones are predominantly medium- to fine-grained, exhibiting subangular to subrounded morphologies with moderate to poor sorting (Fig. 3a). Observed alteration of detrital grains suggests intermediate-short transport distances. Additionally, minor subrounded grains (Fig. 3e) suggest potential sediment recycling or longer transport. The matrix content is low (less than 10 %), predominantly composed of clay-rich or felsic materials, and commonly altered through chloritization.

Quartz (Q) represents the dominant mineral component within the detrital framework, with monocrystalline quartz (Qm) occurring in greater abundance than polycrystalline quartz (Qp). Both quartz types commonly display undulatory extinction and contain fine inclusions of chlorite, zircon, and fluid phases, particularly in monocrystalline grains (Fig. 3d, e). Lithic fragments constitute 38–51 % of the framework composition (Table S2), predominantly comprising sedimentary rock lithics (Ls) and volcanic rock lithics (Lv), including argillaceous rocks, rhyolite, granitic and minor mafic volcanic rocks (e.g., Fig. 3c–f). Feldspar content is relatively low (F = 12–30 %), primarily consisting of plagioclase (Fp), which commonly exhibits polysynthetic twinning and is frequently altered to sericite and kaolinite (Fig. 3e).

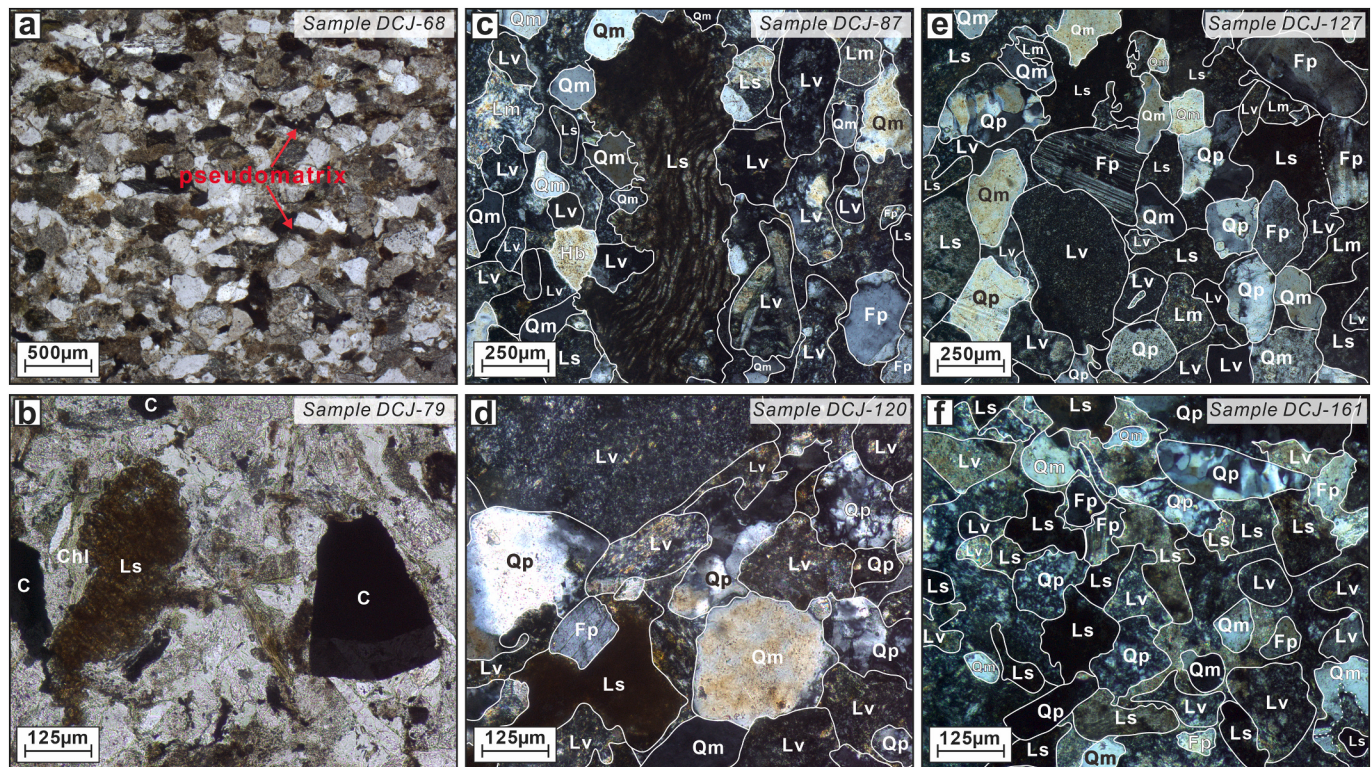


**Fig. 3.** Presents typical microscopic images of the sandstone samples. (a–b) Images under single polarized light show that the detrital grains exhibit a medium- to fine-grained sub-angular texture, containing mud chips and carbonaceous debris. (c–f) Images under crossed polarized light illustrate the grain structures and contact relationships of quartz, feldspar, polycrystalline quartz, and rock fragments.

#### 4.2. Detrital modal

The point-counting data and the results of detrital modal analysis from sandstone thin sections are presented in Table S2 and Fig. 4. Table S2 provides the average compositional values and standard deviations of sandstones. The data are displayed in framework grain assemblages Q-F-L, Qm-F-Lt and Qp-Lsm-Lvm classification diagrams (after Dickinson, 1985).

Lithic fragments represent a major framework constituent (38–51 %; Fig. 4; Table S2). Volcanic lithics are dominated by rhyolite clasts (Fig. 3e, f), with subordinate altered felsic volcanics and basaltic lithic fragments (Fig. 3c, d). Sedimentary lithics exhibit irregular morphologies, primarily comprising argillaceous mudstone and felsic silty mudstone (Fig. 3). Ductile argillaceous lithic embedded between rigid grains form a pseudomatrix texture (Fig. 3a). Metamorphic lithics are rare (Fig. 3c, e). Quartz comprises 30–43 % of framework grains (Q-F-L system). Plagioclase-dominated feldspar constitutes 20 % of the Qm-F-Lt framework, with individual samples ranging from 12 to 30 %. Most of the sample points in the detrital modal analysis diagram cluster in the Transitional Arc and/or Dissected Arc area (Fig. 4a, b). In Qp-Lvm-Lsm diagrams, samples plot within the fields of Arc Orogen Sources (Fig. 4c). Detrital modal analysis indicates that the terrigenous clastics were predominantly derived from the volcanic arc orogenic belt, with minor contributions from recycled orogenic sources.

#### 4.3. Major and trace elements

##### 4.3.1. Major elements

Major and trace element compositions of mudstone and oil shale samples are provided in Table S3. Based on bulk compositions (uncorrected for LOI), mudstones show higher contents of SiO<sub>2</sub>, Fe<sub>2</sub>O<sub>3</sub><sup>T</sup>, MgO, Na<sub>2</sub>O, K<sub>2</sub>O, and P<sub>2</sub>O<sub>5</sub> compared to oil shale samples (Table S3). The significantly higher LOI value in oil shale (26.2 wt%) relative to

mudstone (9.0 wt%) is attributed to its higher organic matter content.

After LOI-free recalculation to 100 % (This chapter and the subsequent sections are based exclusively on the corrected major element compositions for detailed analysis), samples exhibit enriched Al<sub>2</sub>O<sub>3</sub> (22.3 wt%), Fe<sub>2</sub>O<sub>3</sub><sup>T</sup> (6.4 wt%), and TiO<sub>2</sub> (1.0 wt%) relative to the Upper Continental Crust (UCC; Taylor and McLennan, 1995). This Al–Fe–Ti enrichment records advanced chemical weathering promoting residual accumulation of clay minerals and dense minerals (e.g., zircon, iron-bearing mineral), consistent with sandstone petrography.

Additionally, pyritization (Fe<sup>2+</sup> sulfidation) during organic matter decay and adsorption of Fe<sup>3+</sup> species by clays may contribute to Fe enrichment. Plagioclase (Na–Ca-rich) and carbonate minerals (Ca<sup>2+</sup>-bearing) are highly weathering-susceptible. The low Na<sub>2</sub>O and CaO contents support strong chemical weathering, corroborated by scarce plagioclase and carbonates in sandstone thin sections.

##### 4.3.2. Trace elements

All samples exhibit light rare earth elements (LREE) enrichment, with (La/Yb)<sub>n</sub> ratios of 5.25–10.45 (mean 7.53) and display relatively flat heavy rare earth elements (HREE) patterns evidenced by (Gd/Yb)<sub>n</sub> ratios of 1.01–1.62 (mean 1.31). These characteristics define a LREE-enriched pattern analogous to Upper Continental Crust (UCC) and Post-Archean Australian Shale (PAAS), but with moderately elevated HREE concentrations relative to PAAS (Fig. 5a). Oil shale samples exhibit weaker negative Eu anomalies than mudstones, with only two samples showing near-normal values (Eu/Eu<sup>\*</sup> = 0.71–1.11, mean 0.85). Mudstone samples display more pronounced negative Eu anomalies (Eu/Eu<sup>\*</sup> = 0.53–0.75, mean 0.68), closely resembling the PAAS value (Eu/Eu<sup>\*</sup> = 0.65; Taylor and McLennan, 1985). On the UCC-normalized multi-element diagram (Fig. 5b), samples show consistent patterns. Relative to UCC, most samples have Large Ion Lithophile Elements (LILEs) concentrations ranging from slightly depleted (e.g., Rb, Ba, Th) to near-UCC levels, with significant Sr depletion indicative of strong

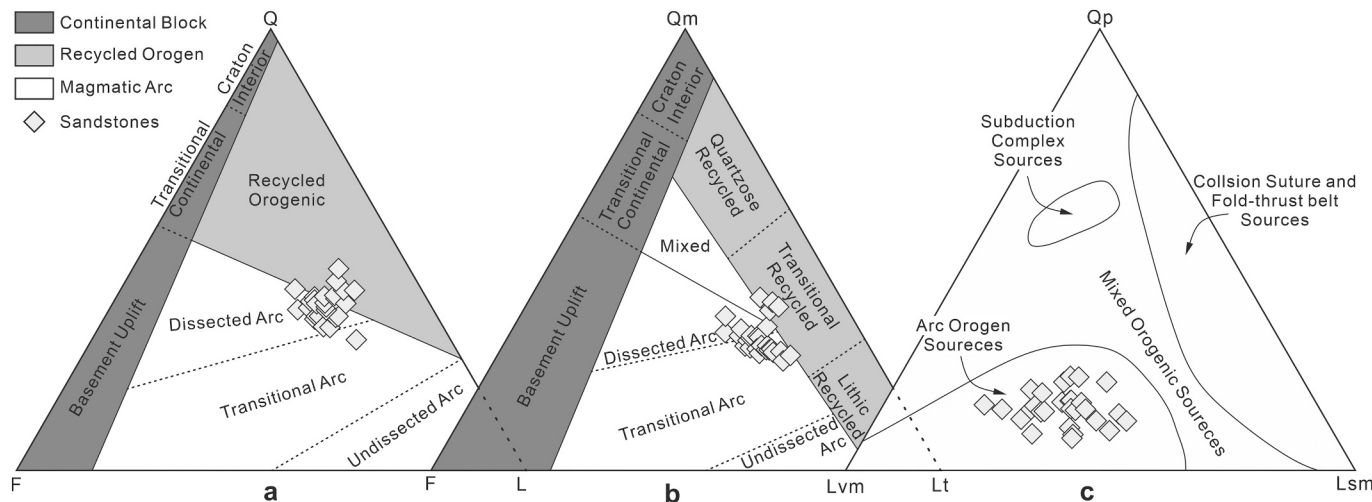


**Fig. 4.** Triangular plots of sandstone framework grain compositions. (a) Q-F-L diagram. (b) Qm-F-Lt diagram (Dickinson et al., 1983). (c) Qp-Lvm-Lsm diagram. Provenance fields are from Dickinson, 1985. For data and abbreviations are shown in Table S2.

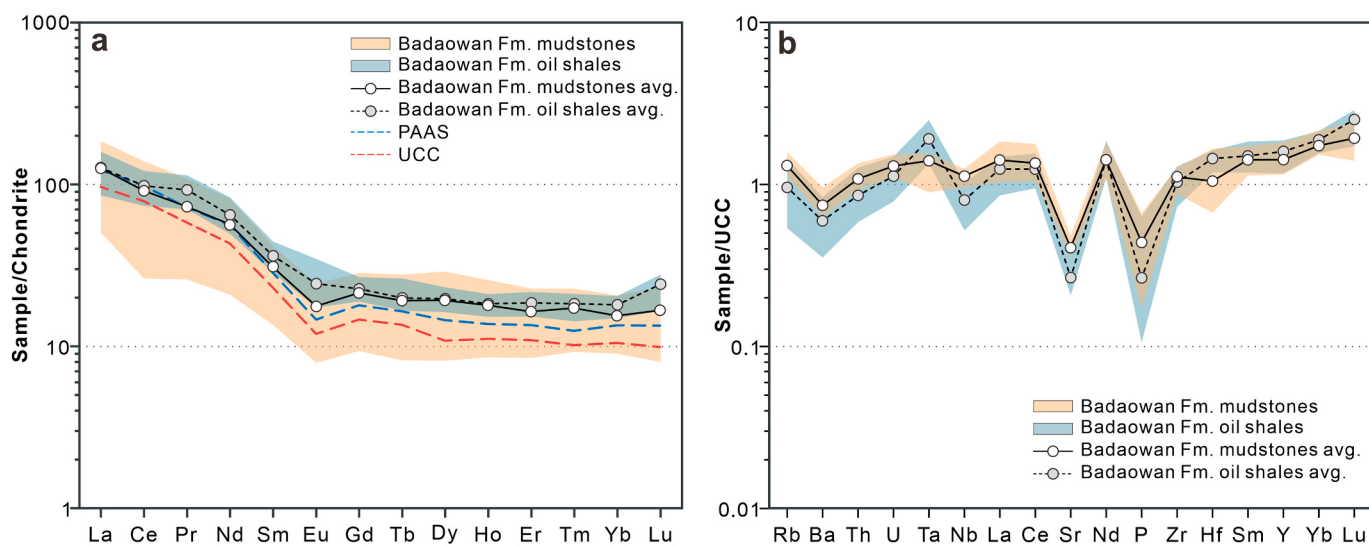


**Fig. 5.** Trace element distribution patterns of the Badaowan Formation. (a) Chondrite-normalized REE patterns (normalization values from Boynton, 1984; PAAS values from Taylor and McLennan, 1985). (b) UCC-normalized multi-element spidergrams (UCC values from Taylor and McLennan, 1995).

chemical weathering. High Field Strength Elements (HFSEs) show relative enrichment in Ta, Y, Yb, and Lu, whereas Zr and Nb concentrations are comparable to or marginally lower than UCC values.

#### 4.4. Geochronology

The U-Pb dating results of detrital zircons are summarized in Table S4. Zircon grains from the sandstone samples are predominantly colorless and prismatic, with a minority exhibiting subrounded to rounded outlines. Grain sizes range from 70 to 230  $\mu\text{m}$ , with length-to-width ratios predominantly ranging from 1:1 to 3:1. Most zircon grains display clear and narrow oscillatory zoning in cathodoluminescence (CL) images, and no discernible xenocrystic cores were detected (Fig. 6c, f). These zircons exhibit high Th/U ratios (all  $> 0.25$  except for one grain; Fig. 6b, e), supporting a magmatic origin (Corfu et al., 2003). Some zircon grains show signs of fracturing, which may be attributed to long-distance transport (Fig. 6c, f). Furthermore, certain zircon grains, particularly those yielding older ages, commonly exhibit dark sector zoning or homogeneous (metamict) domains mantled by bright metamorphic overgrowths, indicating multistage growth or recrystallization.

Two sandstone samples were subjected to LA-ICP-MS U-Pb dating. After filtering for concordance ( $\leq 10\%$  discordance), 144 concordant ages were obtained, revealing similar age distributions between the two samples (Fig. 6). Sample 19XJ-1 (upper Badaowan Formation; 27 m below top; Fig. 2c) yielded 71 concordant ages (250–886 Ma; Fig. 6a). The youngest age is  $250 \pm 14$  Ma ( $2\sigma$ ). Kernel Density Estimation (KDE) plots show a dominant peak at  $\sim 318$  Ma (71 % of grains), with subordinate peaks at  $\sim 401$  Ma (17 %) and  $\sim 504$  Ma (10 %). Two Proterozoic ages (875, 886 Ma) were recorded (Fig. 6b). Sample 19XJ-2 (lower Badaowan Formation; 120 m below top; Fig. 2c) produced 73 concordant ages (252–1444 Ma; Fig. 6d). The youngest single-grain age is  $252 \pm 5$  Ma ( $2\sigma$ ). KDE results indicate a dominant peak at  $\sim 312$  Ma (63 %), minor peaks at  $\sim 415$  Ma (18 %) and  $\sim 507$  Ma (11 %), with additional Neoproterozoic ( $n = 4$ ) and Mesoproterozoic ages (e.g., 1206, 1444 Ma) (Fig. 6e).

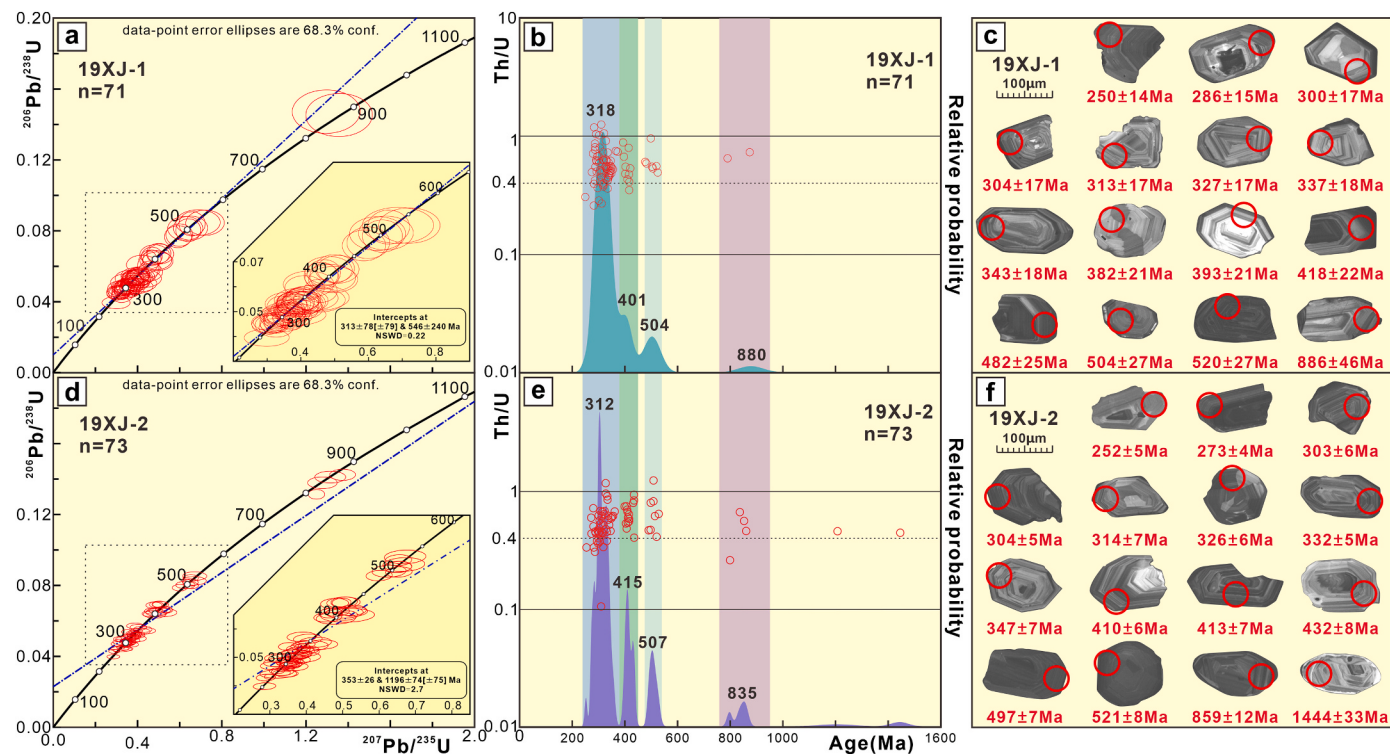


**Fig. 6.** Detrital zircon U-Pb data for Badaowan Formation sandstones. (a, d) Concordia diagrams for samples 19XJ-1 (upper unit) and 19XJ-2 (lower unit). (b, e) Kernel Density Estimation (KDE) plots and Th/U ratios of concordant zircons. Dominant peaks labeled with ages. (c, f) Cathodoluminescence (CL) images of representative zircon grains.

## 5. Discussion

### 5.1. Chemical composition and weathering

Detrital sedimentary rocks, particularly fluvial and lacustrine deposits, preserve robust records of chemical weathering and paleoclimate in their geochemical composition (Fedo et al., 1995; Dinis et al., 2020; Penman et al., 2020; Fu et al., 2023). During sediment transport, alkali and alkaline earth metals (e.g., Na<sup>+</sup>, Ca<sup>2+</sup>, K<sup>+</sup>) are preferentially leached, whereas stable elements (e.g., Al<sup>3+</sup>, Ti<sup>4+</sup>) become enriched in residual phases (Nesbitt and Markovics, 1980; Perri, 2020). Quantitative proxies for paleo-weathering intensity, such as the Chemical Index of Alteration (CIA; Nesbitt and Young, 1982), the Chemical Index of Weathering (CIW; Harnois, 1988), the Plagioclase Index of Alteration (PIA; Fedo et al., 1995), the Weathering Intensity Index of Paker (WIP; Parker, 1970) and the Index of Compositional Variability (ICV; Cox et al., 1995) are popularly used to quantitatively document variations in paleo-weathering intensity and paleoclimate (e.g., Price and Velbel, 2003; Li and Yang, 2010; Cao et al., 2018; Zhao et al., 2025). Before applying these proxies, non-weathering processes—such as diagenesis, sedimentary recycling, and hydraulic sorting—should be systematically assessed to evaluate their potential impact on bulk geochemical signatures (Sun et al., 2022; Fu et al., 2023).

#### 5.1.1. Diagenesis

Prior to geochemical analysis, LOI was excluded from all samples. CaO\* denotes the fraction of calcium bound to silicates. It is defined as the lower value between (CaO – P<sub>2</sub>O<sub>5</sub> × 10/3) and Na<sub>2</sub>O (McLennan, 1993; Fu et al., 2023).

To evaluate diagenetic overprinting, samples were plotted on an A-CN-K ternary diagram (Fig. 7a; Fedo et al., 1995). Oil shale samples exhibit trends subparallel to the A-K join with pronounced displacement toward the A apex, indicating substantial depletion of K-bearing minerals in parent lithologies. Thus, no K<sub>2</sub>O correction was applied.

Conversely, mudstone sample plot trends (Fig. 7a, dashed arrow) align parallel to the A-CN join but deviate from the ideal weathering trend line (Fig. 7a, solid arrow). This divergence implies either preferential leaching of Ca-Na silicates from source rocks (Nesbitt and Young, 1982) or potassic metasomatism during diagenesis (Fedo et al., 1995). The K<sub>2</sub>O content of the mudstone was corrected following the method of Yan et al. (2010), using the formula: K<sub>2</sub>Ocorr = m × (Al<sub>2</sub>O<sub>3</sub> + CaO\* + Na<sub>2</sub>O) / (1 - m), where m represents the intercept value of the extended dashed line of the ideal weathering trend (indicated by the arrowed solid line in Fig. 7a) with the CN-K compositional axis. CIAcorr and WIPcorr were calculated using the corrected K<sub>2</sub>Ocorr. The corrected chemical weathering index data are summarized in Table S3.

#### 5.1.2. Sedimentary differentiation and recycling

Sedimentary differentiation and recycling typically concentrate stable minerals (e.g., quartz) and heavy minerals (e.g., zircon), inducing variations in the content of major and trace element (McLennan et al., 1990; Garzanti et al., 2014). For instance, hydrodynamic sorting during the transport of detrital particles can induce mineralogical and chemical differentiation, such as the SiO<sub>2</sub>/Al<sub>2</sub>O<sub>3</sub> ratio representing grain size and fluid sorting (Garzanti et al., 2010; Guo et al., 2018). Quartz enrichment concomitantly dilutes alkali and alkaline earth element concentrations, resulting in a linear decline in WIP (Garzanti et al., 2014). Furthermore, the ICV index (Cox et al., 1995) and the Zr/Sc (indicating the degree of zircon enrichment) versus Th/Sc (reflecting magmatic differentiation) diagram can also be used to assess sedimentary recycling (McLennan, 1993).

Samples show no significant correlation between the CIAcorr (CIA used for oil shales) and either the SiO<sub>2</sub>/Al<sub>2</sub>O<sub>3</sub> ratio ( $R^2 = 0.07$  for mudstones; 0.41 for oil shales) or the Th/Sc ratio ( $R^2 = 0.12$  for mudstones; 0.12 for oil shales) (Fig. 7b, c). This indicates that variations in the weathering indices are largely independent of hydraulic sorting, particle size, or source rock composition (McLennan, 1993; Bouchez et al., 2011). In contrast, a significant negative correlation exists

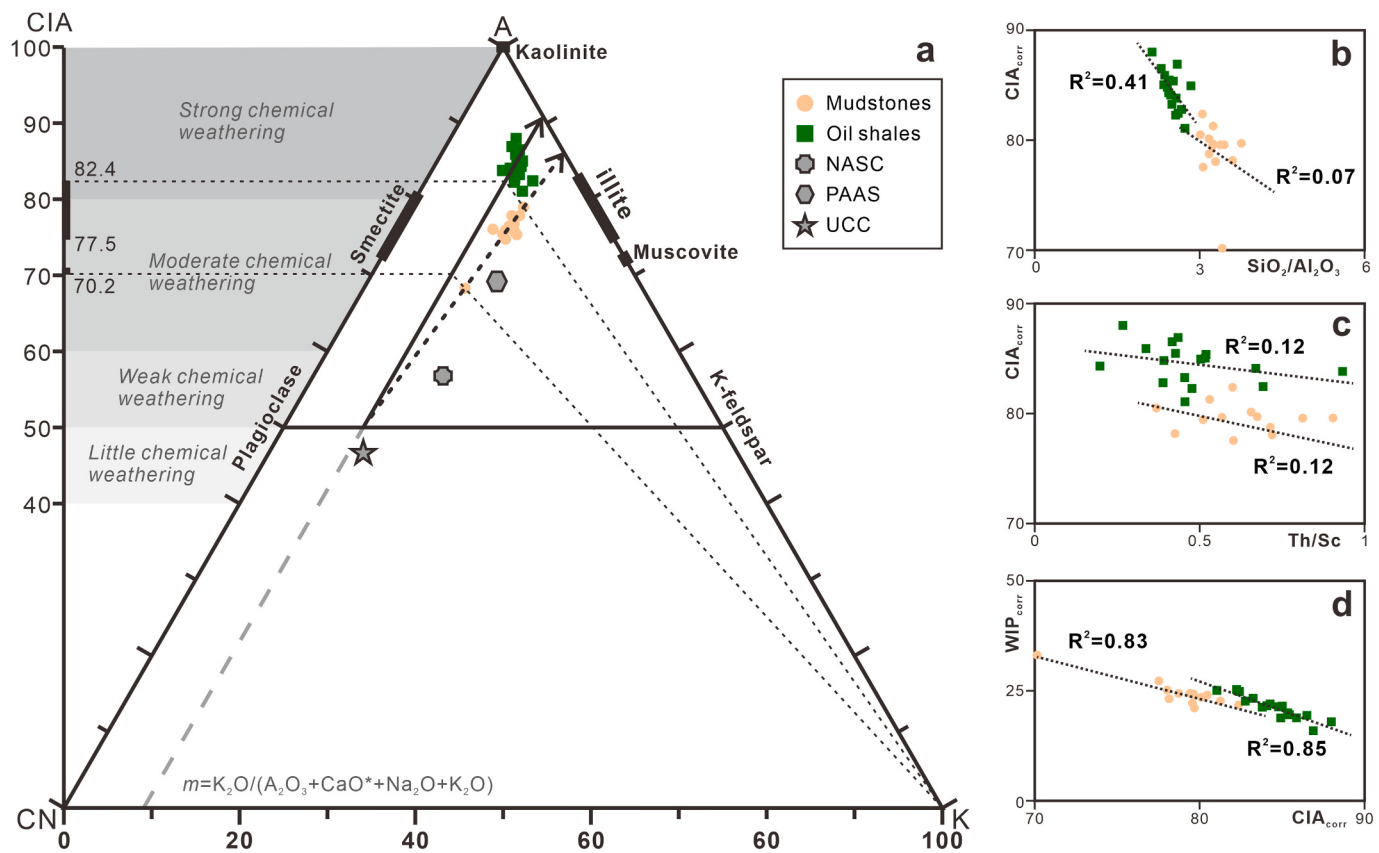


**Fig. 7.** (a) A-CN-K diagram for the mudstone and oil shale samples (Fedo et al., 1995). 'A', 'CN', and 'K' represent ' $Al_2O_3$ ', ' $CaO^* + Na_2O$ ', and ' $K_2O$ ', respectively. Solid- and dashed-line arrows respectively represent the predicted weathering trend and the actual weathering trend for the samples. (b) CIAcorr versus  $SiO_2/Al_2O_3$ , (c) CIAcorr versus Th/Sc, (d) WIPcorr Versus CIAcorr for Badaowan Formation samples; the CIA and WIP of the oil shale samples are the original values.

between CIAcorr and WIPcorr (WIP for oil shales;  $R^2 = 0.83$  for mudstones;  $R^2 = 0.85$  for oil shales; Fig. 7d), suggesting minimal to negligible influence of sedimentary recycling on the compositional trends (Cox et al., 1995). On the Th/Sc versus Zr/Sc diagram, the samples cluster along the Compositional variation trend (Fig. 8a), exhibiting high compositional homogeneity and minimal influence from heavy mineral sorting. This pattern is interpreted to reflect derivation from a primary depositional cycle. Only three mudstone samples show relative Zr enrichment, potentially indicating sedimentary recycling. Mudstone samples exhibit ICV values ranging from 0.74 to 1.00 (mean 0.85), reflecting a mineralogical composition dominated by clay minerals (Cullers and Podkovyrov, 2002). These values are lower than those of PAAS and UCC averages (Table S3), indicating derivation from source terrains of relatively high compositional maturity, likely dominated by felsic rocks (Fedo et al., 1995). In contrast, the oil shale samples display even lower ICV values (mean 0.59). This further indicates their higher compositional maturity compared to the mudstones, suggesting either stronger weathering or derivation from a more compositionally mature (felsic) source region.

#### 5.1.3. Source area weathering

Overall, the samples from the Badaowan Formation exhibit minimal influence from sedimentary differentiation and recycling. Consequently, the chemical weathering signatures inferred from CIAcorr and complementary proxies offer robust constraints. With the exception of one mudstone sample ( $CIA_{corr} = 70.15$ ), the remaining samples display CIAcorr values ranging from 77.54 to 82.37 (mean 78.91; Fig. 7a), indicating that the source rocks experienced moderate to strong chemical weathering. Oil shale samples exhibit relatively high CIA values (81.06–88.00; mean 84.53) and notably low ICV values (mean 0.59), further supporting the interpretation of strong chemical weathering in

their source regions.

#### 5.2. Source rock types

Transition metal elements, high field-strength elements (HFSEs), and REEs in sediments, undergo minimal alteration during chemical weathering and serve as robust indicators for reconstructing source rock composition (Bhatia, 1983; Taylor and McLennan, 1985; McLennan, 1993; Cullers, 2000; Paikaray et al., 2008). Mafic rocks typically exhibit limited REE fractionation with absent-to-neutral or weakly positive Eu anomalies, whereas felsic rocks derived from upper continental crust display light REE enrichment characterized by elevated ( $La/Yb$ )<sub>n</sub> ratios and negative Eu anomalies (Taylor and McLennan, 1985).

Geochemically, mafic rocks are enriched in compatible elements (e.g., Sc, Ni, Cr, Co), while felsic rocks concentrate incompatible elements (e.g., La, Th, Hf, Zr) and REEs (McLennan, 1993; Cullers, 1994; Armstrong-Altrin et al., 2004; Awan et al., 2025b). Consequently, elemental ratios (e.g., Zr/Sc, Th/Sc, La/Sc, La/Th, Co/Th) and bivariate plots provide valuable provenance discriminators. Samples unaffected by significant sedimentary differentiation or recycling yield more accurate constraints on source lithology and tectonic setting.

Certain major elements (e.g., Al, Si, Ti) also demonstrate low mobility during weathering and transport (Sugitani et al., 1996). Aluminum preferentially concentrates in micas, clay minerals, and residual feldspars, whereas titanium is primarily hosted in mafic minerals. The  $Al_2O_3/TiO_2$  ratio thus serves as an effective provenance indicator: values < 14 suggest mafic volcanic sources, while ratios of 19–28 indicate felsic volcanic sources (Girty et al., 1996).

In the Th/Sc versus Zr/Sc bivariate plot (Fig. 8a), most samples plot predominantly within or adjacent to the compositional fields of Tonalite-Trondhjemite-Granodiorite (TTG) suites and Felsic Volcanic

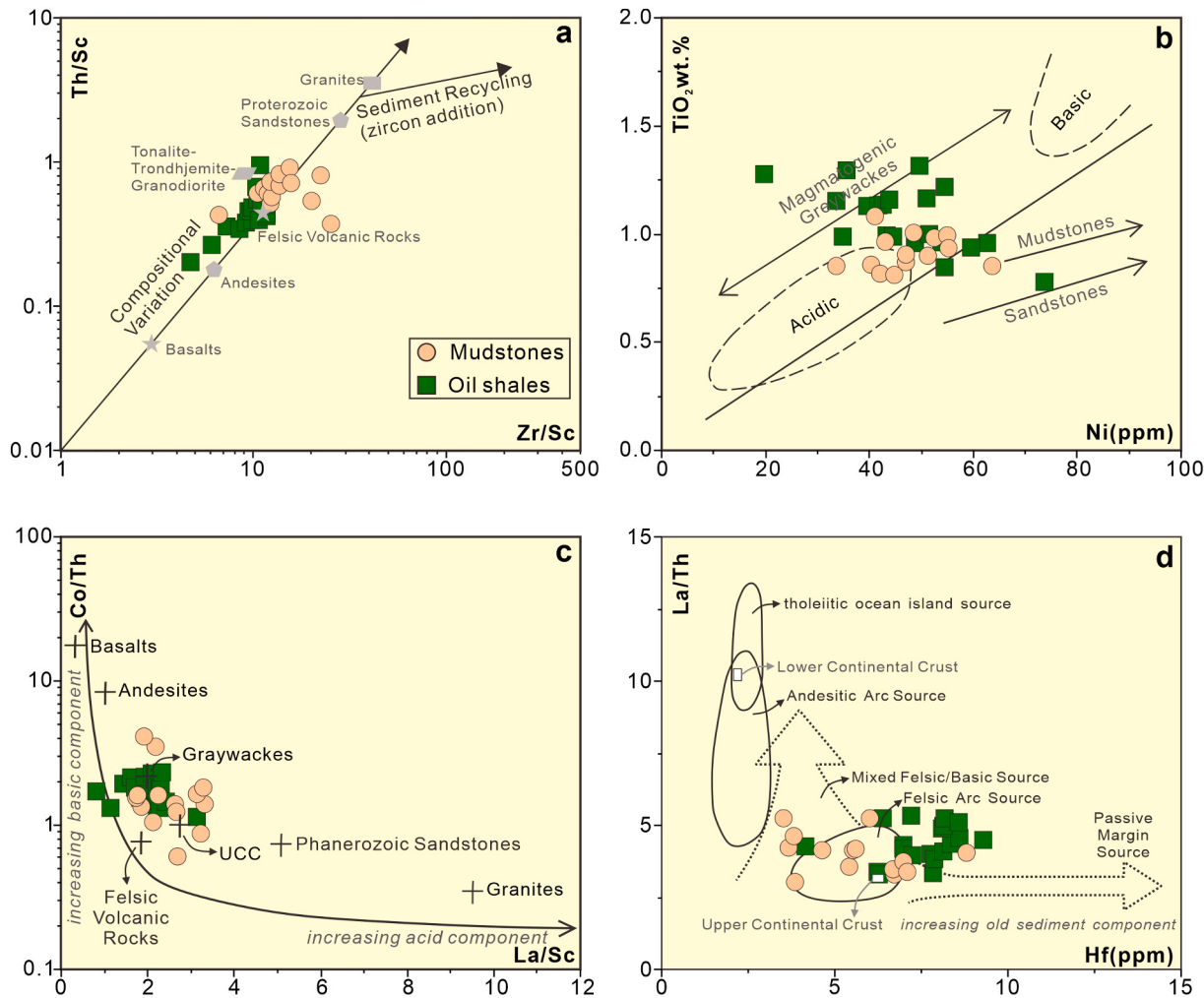


**Fig. 8.** Source rock discrimination diagrams for the Badaowan Formation ( $J_1b$ ) clastic rocks. (a) Plot of  $\text{Th}/\text{Sc}$  versus  $\text{Zr}/\text{Sc}$  (McLennan, 1993). (b) Plot of  $\text{TiO}_2$  versus  $\text{Ni}$  (ppm) (Floyd et al., 1989). (c) Plot of  $\text{Co}/\text{Th}$  versus  $\text{La}/\text{Sc}$  (McLennan, 1993). (d) Plot of  $\text{La}/\text{Th}$  versus  $\text{Hf}$  (ppm) (Floyd and Leveridge, 1987).

Rocks, suggesting that the dominant source lithologies are intermediate to felsic magmatic rocks. The  $\text{TiO}_2$  versus  $\text{Ni}$  diagram reveals that the most samples fall within Acidic domains, with select oil shale samples plotting near the Magmatogenic Greywackes and sedimentary rock fields (Fig. 8b). These patterns align with the average  $\text{Al}_2\text{O}_3/\text{TiO}_2$  ratio of 22.91 for all samples, further supporting a dominantly felsic provenance. Additionally, the oil shale samples contain a relatively high proportion of detrital material derived from long-distance transport or sedimentary recycling processes.

In the  $\text{Co}/\text{Th}$  versus  $\text{La}/\text{Sc}$  diagram, mudstone samples cluster near UCC and Felsic Volcanic Rocks, whereas oil shales trend toward greywacke sources (Fig. 8c). This distribution mirrors the  $\text{La}/\text{Th}-\text{Hf}$  diagram (Fig. 8d): mudstone samples plot near Felsic Arc and Mixed Source regions, while oil shale samples show inputs from old sediment components. As noted in Section 4.3.2, mudstones exhibit LREE-enriched patterns with pronounced negative Eu anomalies, whereas oil shales display weaker Eu anomalies—consistent with these provenance interpretations.

Based on multiple analytical methods, we infer that during mudstone deposition, one or more regions containing felsic volcanic arcs with compositions similar to UCC underwent strong chemical weathering, serving as the primary source of proximal detrital material. The oil shale deposition period was marked by a warmer and more humid climate. In addition to the input of near-source detritus, there was also a contribution of old sediments derived from distant sources with intermediate to felsic magmatic affinities.

### 5.3. Tectonic settings and provenance

#### 5.3.1. Tectonic settings of source area

Elemental compositions and ratios of clastic rocks provide reliable constraints for determining source tectonic settings, with established discrimination diagrams (Bhatia, 1983; Bhatia and Crook, 1986; Roser and Korsch, 1986). However, major elements (notably K, Na, Ca) exhibit high mobility during post-depositional processes. Strong chemical weathering of the Badaowan Formation's source rocks depleted Na and Ca while enriching Al, Ti, Fe, and Mg. This geochemical shift causes samples to plot erroneously near Oceanic Island Arc fields in major-element discriminant diagrams (Fig. 9), contradicting evidence for dominantly felsic arc volcanic sources.

Trace elements offer more robust tectonic proxies due to their weathering resistance. In  $\text{La}-\text{Th}-\text{Sc}$ ,  $\text{Th}-\text{Co}-\text{Zr}/10$ , and  $\text{Th}-\text{Sc}-\text{Zr}/10$  ternary diagrams (Fig. 10a), samples cluster within the Continental Island Arc field. The  $\text{Ti}/\text{Zr}$  vs.  $\text{La}/\text{Sc}$  diagram indicates that the majority of sample points are distributed within the transitional zone between the Oceanic Island Arc and Continental Island Arc fields (Fig. 10b), attributed to weathering-induced  $\text{Ti}/\text{Zr}$  elevation and limited zircon enrichment.  $\text{La}/\text{Y}-\text{Sc}/\text{Cr}$  diagram analysis shows that oil shale samples cluster in the Continental Island Arc field, whereas mudstones with higher  $\text{La}/\text{Y}$  ratios are concentrated in the Passive Margin field (Fig. 10c). During chemical weathering, LREE remain in residual products. Organic matter adsorbs HREE and Y more strongly than LREE (Wang et al., 2023a). Enhanced weathering and higher organic matter content in oil shales

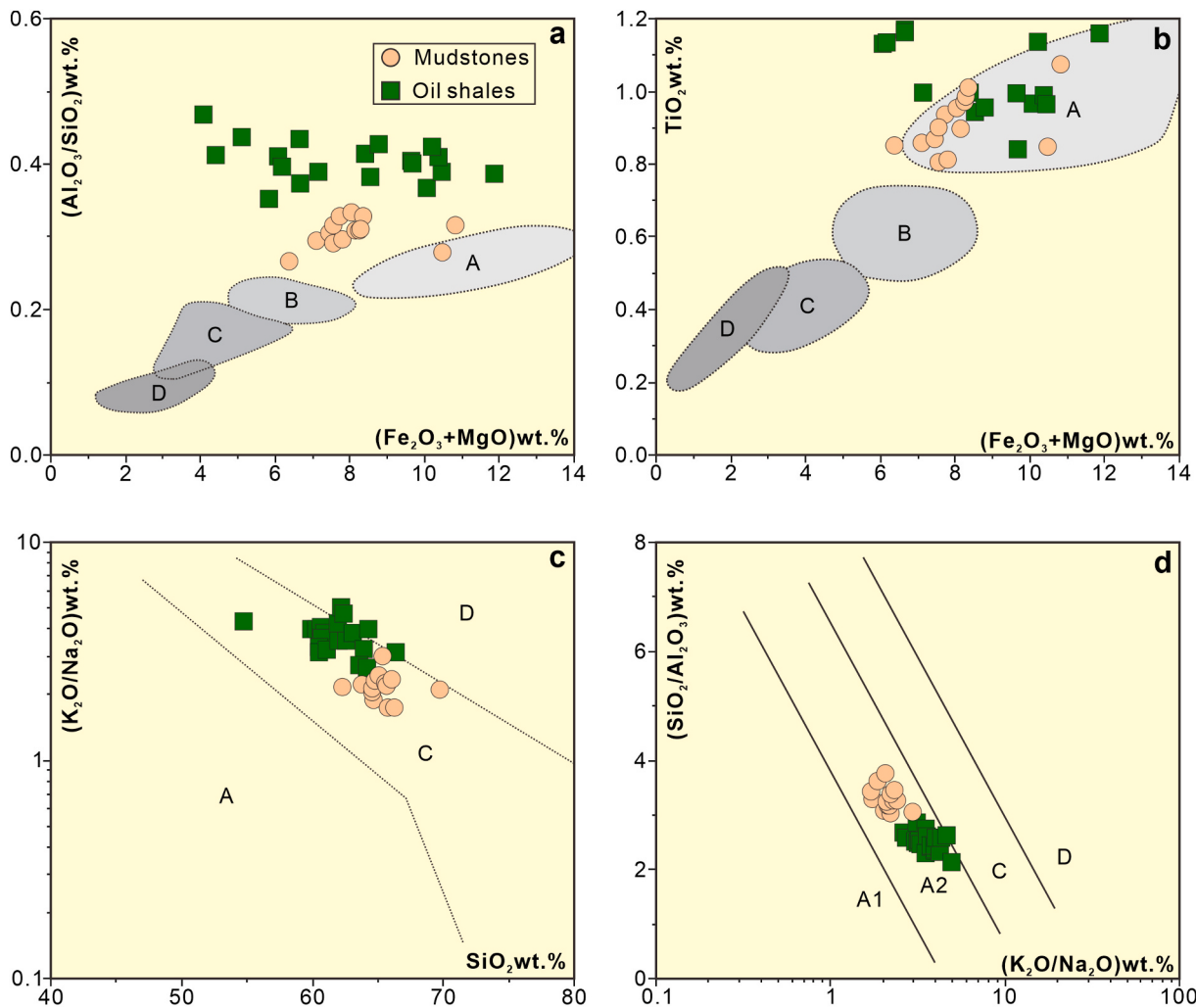


**Fig. 9.** Tectonic discrimination diagrams of major elements for the Badaowan Formation (J<sub>1</sub>b) clastic rocks. (a) Plot of Al<sub>2</sub>O<sub>3</sub>/SiO<sub>2</sub> versus Fe<sub>2</sub>O<sub>3</sub> + MgO. (b) Plot of TiO<sub>2</sub> versus Fe<sub>2</sub>O<sub>3</sub> + MgO (Bhatia, 1983). (c) Plot of SiO<sub>2</sub> versus K<sub>2</sub>O/Na<sub>2</sub>O. (d) Plot of SiO<sub>2</sub>/Al<sub>2</sub>O<sub>3</sub> versus K<sub>2</sub>O/Na<sub>2</sub>O (Roser and Korsch, 1986). A = oceanic island arc; B = continental island arc; C = active continental margin; D = passive margin, and intracratonic; A1 = arc setting, basaltic, and andesitic detritus; A2 = evolved arc setting and felsitic–plutonic detritus.

likely explain the observed geochemical pattern.

The dominant tectonic setting of the Badaowan Formation sediments is interpreted as a continental island arc, as supported by provenance analysis and sandstone detrital modal data (Fig. 4), despite minor inconsistencies among discrimination diagrams.

### 5.3.2. Provenance evolution of the Badaowan Formation

Detrital zircon U-Pb ages from sandstones (samples XJ19-1, XJ19-2) show three predominant populations: 530–480 Ma (peak ~ 505 Ma), 430–390 Ma (peak ~ 410 Ma), and 360–270 Ma (peak ~ 315 Ma; Fig. 6). Precambrian zircons are also present, with Neoproterozoic grains (886–797 Ma) occurring in both samples. The oldest ages (1206 Ma and 1444 Ma) occur only in sample XJ19-2. These Neoproterozoic and Mesoproterozoic zircons match age groups reported in Phanerozoic strata across northern Xinjiang (Long et al., 2012; Zhang et al., 2013b; Wang, 2016; Li et al., 2020), supporting the presence of a Precambrian microcontinental crystalline basement beneath the eastern Junggar terrane. Their rounded shapes, oscillatory zoning, and inherited features (Fig. 6f) suggest magmatic origins and either long-distance transport or multiple sedimentary cycles.

Cambrian igneous rocks are rare in the East Junggar. Magmatic rocks dated to approximately 500 Ma are widespread in southern Mongolia (Kozakov et al., 2002; Yarmolyuk et al., 2008) and the Chinese Altai

Mountains (Yuan et al., 2007; Sun et al., 2009), suggesting that the Cambrian detrital material may have originated from north of the East Junggar. Furthermore, the BOB experienced rift-related subsidence within an intracontinental extensional regime from the Permian through the Middle to Late Triassic (Yang et al., 2022; Gastaldo et al., 2023), during which continental sediments received significant input from the northern Altai (Zhang et al., 2005b). Some Cambrian detrital zircons in the study area may have been recycled from these strata.

The eastern BOB is characterized by extensive Paleozoic volcanic rocks, divided into two main stages: Devonian (400–360 Ma; minor) and Carboniferous to Early Permian (350–270 Ma; major) (Wartes et al., 2002; Wali et al., 2018). No significant magmatic activity has been recorded between 360 and 350 Ma. The Devonian volcanic-sedimentary sequences were formed in a tectonic setting representing an active continental margin and continental island arc, influenced by crustal contamination (Guo et al., 2013; Wang, 2016). Carboniferous–Permian magmatism can be further subdivided into two phases: Early Carboniferous (350–320 Ma) and Late Carboniferous to Early Permian (320–270 Ma). The early phase developed in a continental arc setting, and the later phase transitioned into a post-collisional intra-arc extensional regime, accompanied by localized strike-slip extension (Wali et al., 2018; Zhao et al., 2024). This period is marked by the widespread occurrence of A-type granites and bimodal volcanic rocks (Mao et al., 2014; Du et al.,

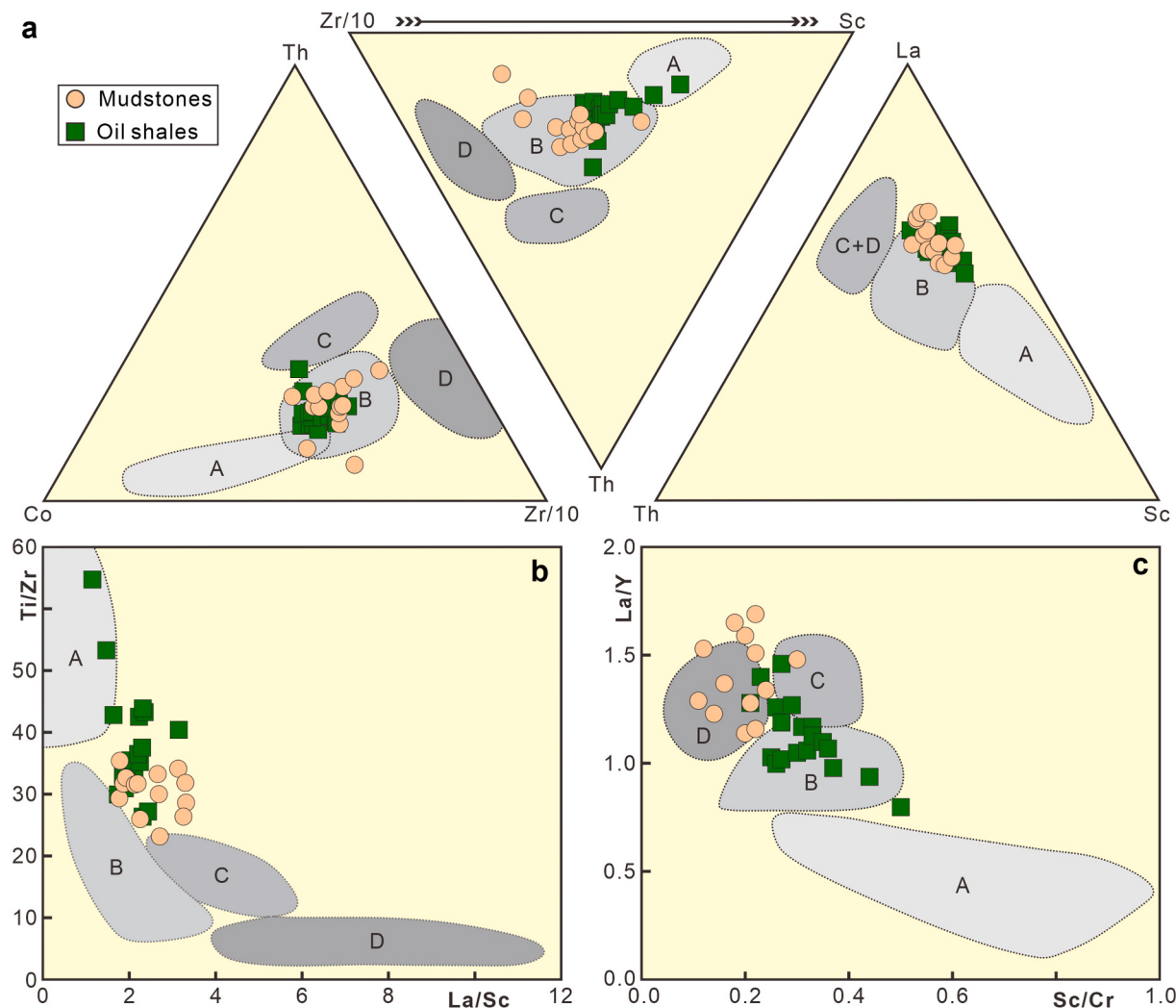


**Fig. 10.** Tectonic discrimination diagrams and ternary plots of trace elements and REEs for clastic rocks (after Bhatia and Crook, 1986). (a) Ternary plot of Th-Co-Zr/10, Th-Sc-Zr/10 and La-Th-Sc. (b) Plot of Ti/Zr versus La/Sc. (c) Plot of La/Y versus Sc/Cr. A = oceanic island arc; B = continental island arc; C = active continental margin; D = passive margin, and intracratonic.

2018). Similarly, the Yemaquan Arc also hosts extensive Paleozoic volcanic rocks (Fig. 1c; BGMRXUAR, 1993; Li et al., 2013), with the Devonian–Carboniferous representing the peak period of magmatic activity. However, this magmatism was temporally discontinuous, particularly lacking records from the Late Devonian (370–360 Ma) (Long et al., 2012). Additionally, minor geological evidence of Ordovician and Silurian magmatic events is also preserved in this region (Long et al., 2012; Li et al., 2020; Xu et al., 2020).

Detrital zircons in sandstone samples exhibit age ranges corresponding to the Devonian and Carboniferous–Early Permian periods, matching with zircon ages from coeval magmatic rocks widely distributed in the East Junggar, including the Bogda Arc and Yemaquan Arc (Fig. 1c; Wang et al., 2010; Cui et al., 2015; Xu et al., 2015; Wang, 2016; Xie et al., 2016; Zhang et al., 2017). Combined with regional paleocurrent data (Zhang et al., 2013a), this suggests that during the Early Jurassic, both Arcs were major sources of Devonian and Carboniferous–Early Permian detrital. The lower sample (XJ19–2) lacks zircon aged 370–360 Ma, while the upper sample (XJ19–1) shows no zircons between 360 and 350 Ma (Table S4). These variations reflect a shift in the magmatic source regions. During early Badaowan deposition, the Yemaquan Arc surrounding the Dachanggou Basin was undergoing regional uplift and erosion, acting as the primary source for the lower section of the Badaowan Formation (Fig. 11a). Later, the climate became

warmer and wetter, enhancing chemical weathering and increasing rainfall. These factors expanded the sediment source area, allowing the more distant Bogda Arc to become the dominant source (Fig. 11b). More Carboniferous zircons in the upper sample (XJ19–1) further confirm this expansion (Fig. 6).

The detrital zircon age spectrum provides key insights into sediment provenance and serves as an indicator of basin tectonic settings. In convergent tectonic regimes, zircon crystallization ages (CAs) typically closely approximate the depositional ages (DAs), while extensional or collisional settings typically contain more older zircons (Cawood et al., 2012). Biostratigraphic data indicate that the Badaowan Formation was deposited during the Early Jurassic (Huang, 2006; Sha et al., 2011). Detrital zircon data reveal a dominant cluster from the Early Carboniferous to Early Permian (360–270 Ma), significantly older than the depositional age and lacks corresponding magmatic zircon records. This suggests an extensional tectonic setting during the Early Jurassic. Moreover, the absence of Triassic zircon ages indicates a post-collisional uplift phase with no magmatic activity. The youngest detrital zircon age does not constrain the maximum depositional age but instead marks the initiation of the Triassic uplift event (non-magmatic uplift) at or before 250 Ma. Additionally, the presence of alluvial fan-braided river coarse clastic deposits in the lower part supports rapid subsidence during early rifting under extension.

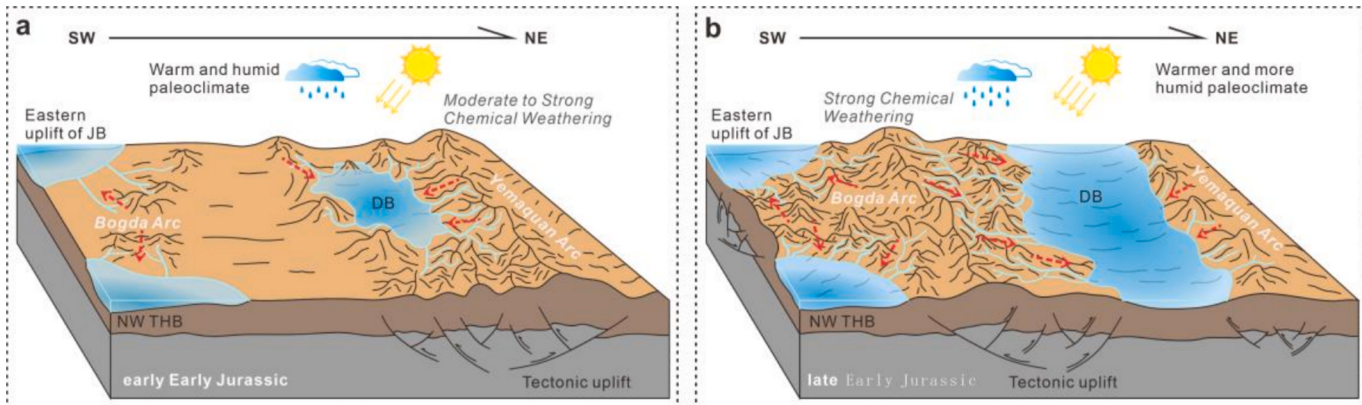


**Fig. 11.** Sketches of the provenance and tectonic evolution in the East Junggar area as described in the text. (a) During the early Early Jurassic, warm and humid paleoclimate led to moderate chemical weathering in the proximal Yemaquan Arc, which was the main source for the lower Badaowan Formation clastic rocks. (b) In the late Early Jurassic, warmer and more humid climate conditions strong chemical weathering in the distal Bogda Arc, making it the dominant source for the upper Badaowan Formation. DB: Dachanggou Basin. THB: Turpan-Hami Basin. JB: Junggar Basin. The apparent size of lakes does not represent their true relative dimensions.

#### 5.4. Early Jurassic source-to-sink system

The Early Jurassic was a key period in the tectonic and climatic development of northern Xinjiang. After the Indosinian Orogeny, the region shifted from compression to extension, leading to basin subsidence and widespread sedimentation (Yang et al., 2015; Deng et al., 2017). The Qiangtang Block collided with Eurasia, and the subduction of the West Mongolian–Okhotsk Ocean caused uplift of the Tianshan, Kalamaili, Bogda, and Harlik ranges between major basins (Vincent and Allen, 2001; Yang et al., 2015). Warm, humid conditions increased weathering and erosion (Ashraf et al., 2010; Sun et al., 2010), supplying sediment for Lower Jurassic deposits. Differential uplift of source areas controlled sediment distribution and depositional variation during this time.

The Junggar Basin's Basin-Range system, bounded by the Tianshan to the south, Zhayier Mountains to the west, and Kalamaili Mountains to the east, began forming in the Early Carboniferous (Wang et al., 2015; Zhang et al., 2020). During the Early Jurassic, the basin's sedimentary center lay in the central depression (Ji et al., 2010; Zhou et al., 2019; Zhou et al., 2022), with sediment sources from surrounding ranges recorded in the rock layers (Wan et al., 2009; Zhou et al., 2019; Gao et al., 2023; Li et al., 2025a, 2025b; Wang et al., 2025). Paleozoic data suggest the Junggar and Turpan-Hami basins were once a single paleobasin, later separated by the uplift of the BOB during the Mesozoic (acting as a tectonic barrier). Researchers debate the uplift timing of the BOB, with proposed phases in the Middle–Late Triassic (Chen et al., 2015; Wang et al., 2018), Early Jurassic (Greene et al., 2001, 2005; Shao et al., 2003; Tang et al., 2014; Ji et al., 2018), and Middle–Late Jurassic (Zhang et al., 2005a; Sun and Liu, 2009). We suggest this discrepancy stems from differences in the basement structure of the BOB. Its eastern and western segments evolved differently during the Carboniferous (Gu et al., 2001), leading to varied uplift patterns in the Mesozoic. In the western BOB, Lower Jurassic strata (Greene et al., 2001; Wang et al., 2008) and paleocurrent data (Hendrix et al., 1992; Zhang et al., 2005a; Li et al., 2007; Zhang et al., 2013b; Zhou et al., 2019) indicate a single sedimentary center, suggesting uplift occurred after the Early Jurassic, likely in the Middle–Late Jurassic (Yang et al., 2015; Zhou et al., 2019). In contrast, the eastern Junggar Basin preserves thin Lower Jurassic deposits showing input from the Kalamaili and eastern BOB (Ji et al., 2010; Tang et al., 2014; Yang et al., 2015; Ji et al., 2018; Zhou et al., 2022). Additional evidence from the Turpan-Hami Basin's northwest—sandstone composition, detrital zircon, and paleocurrent data (Shao et al., 2003; Greene et al., 2005; Qiu et al., 2022)—also supports uplift of the eastern BOB. These findings confirm that the eastern BOB had

topographic relief in the Early Jurassic and acted as a stable sediment source. Our study narrows the uplift timing to the late stage of Badaowan Formation deposition. In eastern East Junggar, Triassic uplift effects continued into the Early Jurassic. At that time, the Santanghu Basin was small, with its sedimentary center in the central area. The Harlik Arc (including the Barkol Basin; Chen et al., 2019) to the southwest supplied sediment to the Santanghu Basin and the northeastern Turpan-Hami Basin. The Yemaquan Arc in the northwest (including the northwest of the Santanghu Basin; Jiang, 2003; Liu, 2010) provided sediment to the Santanghu and Dachanggou Basins.

#### 6. Conclusion

- (1) The geochemical composition of Badaowan Formation clastic rocks indicates minimal influence from sedimentary recycling, grain-size sorting, diagenesis, or supergene alteration. The source rocks underwent moderate to strong chemical weathering.
- (2) Petrological and geochemical data suggest that the Badaowan Formation formed in an intracontinental rift setting linked to post-collisional extension. The sediments were mainly sourced from a mature felsic volcanic arc, indicative of a stable continental island arc tectonic environment.
- (3) Detrital zircon U-Pb ages demonstrate that the main sources of sediment were Paleozoic magmatic rocks from the subduction-related Bogda Arc and Yemaquan Arc of the PAO. Additional contributions originated from Permian rocks in the BOB and northern East Junggar, which supplied Cambrian-aged detritus. Minor inputs of ancient detrital material were provided by Precambrian magmatic rocks and the crystalline basement of microcontinental blocks.
- (4) During the sedimentation of the Badaowan Formation, the regional climate became warmer and more humid, expanding the provenance area. The dominant sediment source shifted from the proximal Yemaquan Arc to the more distal Bogda Arc. Provenance analysis suggests that the eastern Bogda Orogenic Belt had already entered a phase of uplift and erosion by the late Early Jurassic.

Supplementary data to this article can be found online at <https://doi.org/10.1016/j.palaeo.2025.113293>.

#### CRediT authorship contribution statement

Xingxuan Lei: Writing – original draft, Visualization, Methodology,

**Formal analysis, Data curation, Conceptualization.** **Pingchang Sun:** Writing – review & editing, Resources, Funding acquisition. **Junxian Wang:** Resources, Methodology. **Hongliang Dang:** Visualization. **Xuemei Tian:** Data curation. **Zhisheng Luan:** Resources. **Zhuo Wang:** Methodology, Investigation.

## Declaration of competing interest

No conflict of interest arises in the submission of this manuscript, which has been approved by all authors for publication.

## Data availability

The authors confirm that all data necessary for supporting the scientific findings of this paper have been provided.

## Acknowledgements

We are grateful to the Editor-in-Chief, Prof. Howard Falcon-Lang, and three anonymous reviewers for their suggestions and comments, which significantly improved the quality of the manuscript. We acknowledge funding from the National Natural Science Foundation of China (42372125, 41772092, and 41402088), and the research project “Mineral-Fluid-Pore Evolution and Shale Reservoir Classification Evaluation Technology Research” (Grant No. 2021DJ0103) funded by China Petroleum & Natural Gas Corporation (CNPC).

## References

- An, R., Zhao, G.C., Liu, Q., Han, Y.G., 2021. Early Palaeozoic subduction-accretion in East Junggar (NW China): Insights from age, geochemical, and Sr-Nd-Hf isotopic data of andesitic rocks in the northern Yemaquan Arc. *Lithos* 380–381, 105892.
- Andersen, T., 2002. Correction of common lead in U-Pb analyses that do not report Pb-204. *Chem. Geol.* 192, 59–79.
- Armstrong-Altrin, J.S., Lee, Y.I., Verma, S.P., Ramasamy, S., 2004. Geochemistry of sandstones from the Upper Miocene Kudankulam Formation, Southern India: Implications for provenance, weathering, and tectonic setting. *J. Sediment. Res.* 74, 285–297.
- Ashraf, A.R., Sun, Y.W., Sun, G., Uhl, D., Mosbrugger, V., Li, J., Herrmann, M., 2010. Triassic and Jurassic palaeoclimate development in the Junggar Basin, Xinjiang, Northwest China—a review and additional lithological data. *Palaeobio. Palaeoenv.* 90, 187–201.
- Awan, R.S., Liu, B., Li, H.X., Ali, S., Gul, M.A., Zhao, L.S., Khan, A., 2025a. Unlocking paleolatitudinal secrets of the early cretaceous by rare earth element imprints: Implications for seawater chemistry, depositional environments, and paleoclimate in the Talhar Shale, lower Indus Basin Pakistan. *Palaeogeogr. Palaeoclimatol. Palaeoecol.* 671, 112985.
- Awan, R.S., Liu, B., Yasin, Q., Wood, D.A., Rahim, H. ur, Gul, M.A., Ali, S., Iltaf, K.H., Khan, A., 2025b. Paleoenvironmental conditions and key drivers of organic matter accumulation in the early cretaceous Talhar Shale, lower Indus Basin, Pakistan. *J. Asian Earth Sci.* 292, 106716.
- Bai, Y.Y., Wang, J.X., Liu, Z.J., 2023. Characteristics, Genesis, and Hydrocarbon Aspects of Lacustrine Siderite-Rich Marl (early Jurassic): A case study in the dachanggou basin, Xinjiang, Northwest China. *ACS Earth Space Chem.* 7, 338–349.
- BGMRXUAR, 1993. Regional Geology of Xinjiang Uygur Autonomous Region. Geological Publishing House, Beijing (in Chinese with English abstract).
- Bhatia, M.R., 1983. Plate tectonics and geochemical composition of sandstones. *J. Geol.* 91 (6), 611–627.
- Bhatia, M.R., 1985. Rare earth element geochemistry of Australian Paleozoic graywackes and mudrocks: Provenance and tectonic control. *Sediment. Geol.* 45 (1–2), 97–113.
- Bhatia, M.R., Crook, K.A.W., 1986. Trace element characteristics of graywackes and tectonic setting discrimination of sedimentary basins. *Contrib. Mineral. Petr.* 92 (2), 181–193.
- Bouchez, J., Gaillardet, J., France-Lanord, C., Maurice, L., Dutra-Maia, P., 2011. Grain size control of river suspended sediment geochemistry: clues from Amazon River depth profiles. *Geochem. Geophys. Geosyst.* 12 (3).
- Boynton, W.V., 1984. Cosmochemistry of the rare earth elements: Meteorite studies. In: Henderson, P. (Ed.), Developments in geochemistry, 2. Department of Mineralogy, London, pp. 63–114. British Museum (Natural History).
- Cao, Y., Song, H., Algeo, T.J., Chu, D., Du, Y., Tian, L., Wang, Y., Tong, J., 2018. Intensified chemical weathering during the Permian-Triassic transition recorded in terrestrial and marine successions. *Palaeogeogr. Palaeoclimatol. Palaeoecol.* 519, 166–177.
- Carroll, A.R., 1998. Upper Permian lacustrine organic facies evolution, southern Junggar Basin, NW China. *Org. Geochem.* 28, 649–667.
- Cawood, P.A., Hawkesworth, C.J., Dhuime, B., 2012. Detrital Zircon Record and Tectonic setting. *Geology* 40, 875–878.
- Charvet, J., Shu, L.S., Laurent-Charvet, S., 2007. Paleozoic structural and geodynamic evolution of eastern Tianshan (NW China): welding of the Tarim and Junggar plates.  *Episodes* 30(3), 162–186.
- Charvet, J., Shu, L.S., Laurent-Charvet, S., Wang, B., Faure, M., Cluzel, D., Chen, Y., Jong, K.D., 2011. Palaeozoic tectonic evolution of the Tianshan belt, NW China. *Sci. China Earth Sci.* 54, 166–184.
- Chen, B., Jahn, B.M., 2004. Genesis of post-collisional granitoids and basement nature of the Junggar Terrane, NW China: Nd-Sr isotope and trace element evidence. *J. Asian Earth Sci.* 23 (5), 691–703.
- Chen, K., Lin, W., Wang, Q.C., 2015. The Bogeda Shan uplifting: evidence from multiple phases of deformation. *J. Asian Earth Sci.* 99, 1–12.
- Chen, Y., Wang, G.C., Zhao, X., Wang, Y.B., Ji, J.L., Cao, K., Shen, T., Zhang, P., Wang, A., 2019. Evolution of the Barkol Basin, eastern Tian Shan, and its geodynamic background. *Int. J. Earth Sci.* 108, 1253–1271.
- Condie, K.C., 1991. Another look at rare earth elements in shales. *Geochim. Cosmochim. Acta* 55 (9), 2527–2531.
- Condie, K.C., 1993. Chemical composition and evolution of the upper continental crust: contrasting results from surface samples and shales. *Chem. Geol.* 104 (1–4), 1–37.
- Corfu, F., Hanchar, J.M., Hoskin, P.W., Kinny, P., 2003. Atlas of zircon textures. *Rev. Mineral. Geochem.* 53 (1), 469–500.
- Cox, R., Lowe, D.R., Cutters, R.L., 1995. The influence of sediment recycling and basement composition on evolution of mudrock chemistry in the southwestern United States. *Geochim. Cosmochim. Acta* 59, 2919–2940.
- Cui, F., Wang, X., Xu, X., Ma, Z., Zhu, X., Sun, J., 2015. Geochronology and genesis of the diabase dykes from Qijiaojing-Balkun area in Eastern Tianshan Mountain. *Northwest. Geol.* 48, 43–56 (in Chinese with English abstract).
- Cutters, R.L., 1994. The controls on the major and trace element variation of shales, siltstones, and sandstones of Pennsylvanian-Permian age from uplifted continental blocks in Colorado to platform sediment in Kansas, USA. *Geochim. Cosmochim. Acta* 58 (22), 4955–4972.
- Cutters, R.L., 2000. The geochemistry of shales, siltstones and sandstones of Pennsylvanian-Permian age, Colorado, USA: Implications for provenance and metamorphic studies. *Lithos* 51, 305–327.
- Cutters, R.L., Podkorytov, V.N., 2002. The source and origin of terrigenous sedimentary rocks in the Mesoproterozoic Ui group, southeastern Russia. *Precambrian Res.* 117, 157–183.
- Deng, S.H., Lu, Y.Z., Fan, R., Pan, Y.H., Cheng, X.S., Fu, G.B., Wang, Q.F., Pan, H.Z., Shen, Y.B., Wang, Y.Q., Zhang, H.C., Jia, C.K., Duan, W.Z., Fang, L.H., 2010. The Jurassic System of Northern Xinjiang, China. University of Science and Technology of China Press, Hefei (in Chinese with English abstract).
- Deng, S.H., Lu, Y.Z., Zhao, Y., Fan, R., Wang, Y.D., Yang, X.J., Li, X., Sun, B.N., 2017. The Jurassic palaeoclimate regionalization and evolution of China. *Earth Sci. Front.* 24, 106–142 (in Chinese with English abstract).
- Dickinson, W.R., 1985. Interpreting Provenance Relations from Detrital Modes of Sandstones. In: Zuffa, G.G. (Ed.), Provenance of Arenites. Springer, Dordrecht, pp. 333–361.
- Dickinson, W.R., Gehrels, G.E., 2009. Use of U-Pb ages of detrital zircons to infer maximum depositional ages of strata: a test against a Colorado Plateau Mesozoic database. *Earth Planet. Sc. Lett.* 288 (1–2), 115–125.
- Dickinson, W.R., Beard, L.S., Brakenridge, G.R., Erjavec, J.L., Ferguson, R.C., Inman, K. F., Knepp, R.A., Lindberg, F.A., Ryberg, P.T., 1983. Provenance of north American Phanerozoic sandstones in relation to tectonic setting. *Geol. Soc. Am. Bull.* 94 (2), 222–235.
- Denis, P.A., Garzanti, E., Hahn, A., Vermeesch, P., Cabral-Pinto, M., 2020. Weathering indices as climate proxies: A step forward based on Congo and SW African river muds. *Earth Sci. Rev.* 556, 109873.
- Dong, L.H., Qu, X., Zhu, Z.X., Zhang, L.C., 2010. Tectonic evolution and metallogenesis of Xinjiang, China. *Xinjiang Geol.* 28, 351–357 (in Chinese with English abstract).
- Du, L., Long, X.P., Yuan, C., Zhang, Y.Y., Huang, Z.Y., Wang, X.Y., Yang, Y.H., 2018. Mantle contribution and tectonic transition in the Aqishan–Yamansu Belt, Eastern Tianshan, NW China: Insights from geochronology and geochemistry of Early Carboniferous to Early Permian felsic intrusions. *Lithos* 304–307, 230–244.
- Fedo, C.M., Nesbitt, H.W., Young, G.M., 1995. Unraveling the effects of potassium metasomatism in sedimentary rocks and paleosols, with implications for paleoweathering conditions and provenance. *Geology* 23, 921–924.
- Floyd, P.A., Leveridge, B.E., 1987. Tectonic environment of the Devonian Gramscatho basin, South Cornwall: framework mode and geochemical evidence from turbiditic sandstones. *J. Geol. Soc. London* 144, 531–542.
- Floyd, P.A., Winchester, J.A., Park, R.G., 1989. Geochemistry and tectonic setting of Lewisian clastic metasediments from the early Proterozoic Loch Maree Group of Gairloch, NW Scotland. *Precambrian Res.* 45 (1–3), 203–214.
- Fu, H., Jian, X., Pan, H., 2023. Bias in sediment chemical weathering intensity evaluation: a numerical simulation study. *Earth Sci. Rev.* 246, 104574.
- Gao, J.Y., Zhang, G.L., Li, S.T., Guo, R.C., Zeng, Z.P., Cheng, S.W., Xue, Z.L., Li, L., Zhou, H.L., Liu, H.L., Liu, F.R., 2023. Provenance of the lower Jurassic Badaowan and Sangonghe Formations in Dongdaohaizi Depression, Junggar Basin, and its Constraint on the Karamaili Ocean. *J. Mar. Sci. Eng.* 11, 1375.
- Garzanti, E., Ando, S., France-Lanord, C., Vezzoli, G., Censi, P., Galy, V., Najman, Y., 2010. Mineralogical and chemical variability of fluvial sediments 1. Bedload sand (Ganga–Brahmaputra, Bangladesh). *Earth Planet. Sci. Lett.* 299, 368–381.
- Garzanti, E., Padoan, M., Setti, M., López-Galindo, A., Villa, I.M., 2014. Provenance versus weathering control on the composition of tropical river mud (southern Africa). *Chem. Geol.* 366, 61–74.
- Gastaldo, R.A., Wan, M., Yang, W., 2023. The taphonomic character, occurrence, and persistence of upper Permian lower Triassic plant assemblages in the mid-paleolatitudes, Bogda Mountains, western China. *Palaios* 38 (1), 1–21.

- Geslin, J.K., Karl, L.P., Mark, F.C., 1999. High-precision provenance determination using detrital-zircon ages and petrography of Quaternary sands on the eastern Snake River Plain, Idaho. *Geology* 27 (4), 295–298.
- Girty, G.H., Ridge, D.L., Knaack, C., Johnson, D., Al-Riyami, R.K., 1996. Provenance and depositional setting of Paleozoic chert and argillite, Sierra Nevada, California. *J. Sediment. Res.* 66, 107–118.
- Govindaraju, K., 1994. 1994 compilation of working values and sample description for 383 geostandards. *Geostand. Newslett.* 18, 1–158.
- Greene, T.J., Carroll, A.R., Hendix, M.S., Graham, S.A., Wartes, M.A., Abbink, O.A., 2001. Sedimentary record of Mesozoic deformation and inception of the Turpan-Hami basin, north-West China. *Geol. Soc. Am. Bull.* 194, 317–340.
- Greene, T.J., Carroll, A.R., Wartes, M., Graham, S.A., Wooden, J.L., 2005. Integrated Provenance Analysis of a complex Orogenic Terrane: Mesozoic Uplift of the Bogda Shan and Inception of the Turpan-Hami Basin, NW China. *J. Sediment. Res.* 75, 251–267.
- Gu, L.X., Hu, S.X., Yu, C.S., Wu, C.Z., Yan, Z.F., 2001. Initiation and evolution of Bogda subduction-torn-type rift. *Acta Petrol. Sin.* 17, 585–597 (in Chinese with English abstract).
- Guo, X.J., Zhang, C.L., Li, L., Zhao, J., 2013. Determination of Silurian granitic plutons in the Balikun area, Xinjiang and its implications. *Chinese J. Geol.* 48 (4), 1050–1068 (in Chinese with English abstract).
- Guo, Y.L., Yang, S.Y., Su, N., Li, C., Yin, P., Wang, Z.B., 2018. Revisiting the effects of hydrodynamic sorting and sedimentary recycling on chemical weathering indices. *Geochim. Cosmochim. Acta* 227, 48–63.
- Harnois, L., 1988. The CIW index: a new chemical index of weathering CIW. *Sediment. Geol.* 55, 319–322.
- Hendrix, M.S., Graham, S.A., Carroll, A.R., Sobel, E.R., McKnight, C.L., Schulein, B.J., Wang, Z.X., 1992. Sedimentary record and climatic implications of recurrent deformation in the Tian Shan: evidence from Mesozoic strata of the North Tarim, south Junggar, and Turpan basins, Northwest China. *Geol. Soc. Am. Bull.* 104 (1), 53–79.
- Holail, H.M., Moghazi, A.K.M., 1998. Provenance, tectonic setting and geochemistry of greywackes and siltstones of the late Precambrian Hammamat Group, Egypt. *Sediment. Geol.* 116 (3–4), 227–250.
- Huang, G., Niu, G.Z., Zhang, Z.W., Wang, X.L., Xu, X.Y., 2013. Discovery of ~4.0 Ga detrital zircons in the Aermantai ophiolitic mélange, East Junggar, Northwest China. *Chin. Sci. Bull.* 58 (30), 3645–3663.
- Huang, P., 2006. Sporopollen assemblages from the Haojiagou and Badaowan formations at the Haojiagou section of Urumqi, Xinjiang and their stratigraphical significance. *Acta Micropalaeontologica Sinica* 23, 235–275 (in Chinese with English abstract).
- Ingersoll, R.V., Bullard, T.F., Ford, R.L., Grimm, J.P., Pickle, J.D., Sares, S.W., 1984. The effect of grain size on detrital modes: a test of the Gazzi–Dickinson point-counting method. *J. Sediment. Res.* 54 (1), 103–116.
- Jahn, B.M., Wu, F.Y., Chen, B., 2000. Granitoids of the Central Asian Orogenic Belt and continental growth in the Phanerozoic. *Earth Env. Sci. T. R. So.* 91 (1–2), 181–193.
- Ji, H.J., Tao, H.F., Wang, Q., Qiu, Z., Ma, D.X., Qiu, J.L., Liao, P., 2018. Early to Middle Jurassic tectonic evolution of the Bogda Mountains, Northwest China: evidence from sedimentology and detrital zircon geochronology. *J. Asian Earth Sci.* 153, 57–74.
- Ji, Y.L., Zhou, Y., Kuang, J., Wan, L., Zhang, R., Lu, C.H., 2010. The formation and evolution of Chepaizi-Mosuowan paleo-uplift and its control on the distributions of sedimentary facies in the Junggar Basin. *Sci. China Earth Sci.* 53, 818–831.
- Jiang, G.B., 2003. Research on the Jurassic Sedimentary System in the Santanghu Basin. Dissertation for Master's Degree. Department of Geology, Shanxi. Northwest University (in Chinese with English abstract).
- Kozakov, I.K., Salnikova, E.B., Khain, E.V., Kovach, V.P., Berezhnaya, N.G., Yakovleva, N.G., Plotkina, Y.V., 2002. Early Caledonian crystalline rocks of the Lake zone, Mongolia: stages and tectonic environments as deduced from U-Pb and Sm-Nd isotopic data. *Geotectonics* 36, 156–166.
- Laurent-Charvet, S., Charvet, J., Shu, L.S., Ma, R.S., Lu, H.F., 2002. Palaeozoic late collisional strike-slip deformations in Tianshan and Altay, eastern Xinjiang, NW China. *Terra Nova* 14 (4), 249–256.
- Li, C., Yang, S., 2010. Is chemical index of alteration (CIA) a reliable proxy for chemical weathering in global drainage basins? *Am. J. Sci.* 310, 111–127.
- Li, D., He, D.F., Sun, M., Zhang, L., 2020. The Role of arc-arc collision in accretionary orogenesis: Insights from ~ 320 Ma tectono-sedimentary transition in the Karamaili Area, NW China. *Tectonics* 39 (1), e2019TC005623.
- Li, F.R., Zhang, Z., Zhao, C., Han, J.Q., Liu, J.Y., Guo, Y.Y., Tang, X.Y., Su, C., Chang, X., Wu, T., 2025b. Petrography and Geochemistry of lower Jurassic Sandstones in the Eastern Junggar Basin: Implications for Provenance and Tectonic setting. *Minerals* 15, 279.
- Li, H.X., Liu, B., Liu, X.Z., Meng, L., Cheng, L.J., Wang, H.X., 2019. Mineralogy and inorganic geochemistry of the Es4 shales of the Damintun Sag, northeast of the Bohai Bay Basin: Implication for depositional environment. *Mar. Petrol. Geol.* 110, 886–900.
- Li, H.X., Liu, B., Jiang, Q.C., Xu, C.L., Wang, Z.G., Awan, R.S., Lu, H.F., Guo, L., 2025a. Elemental geochemistry of the Aalenian (Middle Jurassic) shales from the northeastern Sichuan Basin: evidence for provenance, climate oscillations and organic matter accumulation mechanism. *Mar. Petrol. Geol.* 180, 107485.
- Li, J.Y., Yang, T.N., Li, Y.P., Zhu, Z.X., 2009. Geological features of the Karamaili faulting belt, eastern Junggar region, Xinjiang, China and its constraints on the reconstruction of late Paleozoic Ocean-continent framework of the Central Asian region. *Geol. Bull. China* 28 (12), 1817–1826 (in Chinese with English abstract).
- Li, W., Hu, J.M., Li, D.P., Liu, J.X., Sun, Y.P., Liang, J.W., 2007. Analysis of the late Paleozoic and Mesozoic paleocurrents and its constructional significance of the northern Bogdashan, Xinjiang. *Acta Sedimentol. Sin.* 25, 283–292.
- Li, W., Liu, Y.Q., Dong, Y.P., Zhou, X.H., Liu, X.M., Li, H., Fan, T.T., Zhou, D.W., Xu, X.Y., Chen, J.L., 2013. The geochemical characteristics, geochronology and tectonic significance of the Carboniferous volcanic rocks of the Santanghu area in northeastern Xinjiang, China. *Sci. China Earth Sci.* 56 (8), 1318–1333.
- Liu, B., Bechtel, A., Gross, D., Fu, X., Li, X., Sachsenhofer, R.F., 2018. Middle Permian environmental changes and shale oil potential evidenced by high-resolution organic petrology, geochemistry and mineral composition of the sediments in the Santanghu Basin, Northwest China. *Int. J. Coal Geol.* 185, 119–137.
- Liu, Y., 2010. The Tectonic Evolution in the Santanghu Basin and its Relationship to Oil and Gas. Dissertation for Master's Degree. School of Earth Sciences and Resources, China University of Geosciences (in Chinese with English abstract).
- Liu, Y.S., Hu, Z.C., Zong, K.Q., Gao, C.G., Gao, S., Xu, J., Chen, H.H., 2010. Reappraisal and refinement of zircon U-Pb isotope and trace element analyses by LA-ICP-MS. *Chin. Sci. Bull.* 55 (15), 1535–1546.
- Long, X.P., Yuan, C., Sun, M., Safonova, I., Xiao, W.J., Wang, Y.J., 2012. Geochemistry and U-Pb detrital zircon dating of Paleozoic graywackes in East Junggar, NW China: insights into subduction-accretion processes in the southern Central Asian Orogenic Belt. *Gondw. Res.* 21 (2–3), 637–653.
- Ludwig, K., 2003. Users manual for Isoplots/Ex version 3.00 – A Geochronology Toolkit for Microsoft Excel, no. 4. Berkeley: Berkeley Geochronological Center, Special Publication.
- Luo, J., Xiao, W.J., Wakabayashi, J., Han, C.M., Zhang, J.E., Wan, B., Ao, S.J., Zhang, Z.Y., Tian, Z.H., Song, D.F., Chen, Y.C., 2017. The Zhaheba ophiolite complex in Eastern Junggar (NW China): Long lived supra-subduction zone ocean crust Formation and its implications for the tectonic evolution in southern Altaiids. *Gondw. Res.* 43, 17–40.
- Mao, Q.G., Xiao, W.J., Fang, T.H., Windley, B.F., Sun, M., Ao, S.J., Zhang, J.E., Huang, X.K., 2014. Geochronology, geochemistry and petrogenesis of early Permian alkaline magmatism in the Eastern Tianshan: Implications for tectonics of the Southern Altaiids. *Lithos* 190–191, 37–51.
- McLennan, S.M., 1993. Weathering and global denudation. *J. Geol.* 101, 295–303.
- McLennan, S.M., Taylor, S.R., McCulloch, M.T., Maynard, J.B., 1990. Geochemical and Nd-Sr isotopic composition of deep-sea turbidites: Crustal evolution and plate tectonic associations. *Geochim. Cosmochim. Acta* 54, 2015–2050.
- Mu, Y.L., Tian, R.S., Fu, Y., Yang, L., Hu, J., 2024. Sedimentary provenance and paleogeographic environment of a Mississippian coal-bearing unit in South China: Constraints from detrital zircon U-Pb ages and sedimentologic and geochemical evidence. *Palaeogeogr. Palaeoclimatol. Palaeoecol.* 656, 112605.
- Nesbitt, H.W., Markovics, G., 1980. Chemical processes affecting alkalis and alkaline earths during continental weathering. *Geochim. Cosmochim. Acta* 44, 1659–1666.
- Nesbitt, H.W., Young, G.M., 1982. Early Proterozoic climates and plate motions inferred from major element chemistry of lutes. *Nature* 299, 715–717.
- Paikaray, S., Banerjee, S., Mukherji, S., 2008. Geochemistry of shales from the Paleoproterozoic to Neoproterozoic Vindhyan Supergroup: implications on provenance, tectonics and paleoweathering. *J. Asian Earth Sci.* 32, 34–48.
- Parker, A., 1970. An index of weathering for silicate rocks. *Geol. Mag.* 107, 501–504.
- Pearce, J.A., 1983. Role of the sub-continental lithosphere in magma genesis at active continental margins. In: Hawkesworth, C.J., Norry, M.J. (Eds.), *Continental Basalts and Mantle Xenoliths*. Shiva Publications, Nantwich, Cheshire, pp. 230–249.
- Penman, D.E., Rogenstein, J.K.C., Ibarra, D.E., Winnick, M.J., 2020. Silicate weathering as a feedback and forcing in Earth's climate and carbon cycle. *Earth Sci. Rev.* 209, 103298.
- Perri, F., 2020. Chemical weathering of crystalline rocks in contrasting climatic conditions using geochemical proxies: an overview. *Palaeogeogr. Palaeoclimatol. Palaeoecol.* 556, 109873.
- Price, J.R., Velbel, M.A., 2003. Chemical weathering indices applied to weathering profiles developed on heterogeneous felsic metamorphic parent rocks. *Chem. Geol.* 202, 397–416.
- Qiu, Z., Zou, C.N., Mills, B.J.W., Xiong, Y.J., Tao, H.F., Lu, B., Liu, H.L., Xiao, W.J., Poulton, S.W., 2022. A nutrient control on expanded anoxia and global cooling during the late Ordovician mass extinction. *Commun. Earth Environ.* 3, 82.
- Rahim, Y., Li, H., 2025. Depositional age and provenance of the Maziping Group, South China: evidence from detrital zircon U-Pb dating and whole-rock geochemistry. *Palaeogeogr. Palaeoclimatol. Palaeoecol.* 676, 113134.
- Ren, R., Han, B.F., Xu, Z., Zhou, Y.Z., Liu, B., Zhang, L., Chen, J.F., Su, L., Li, J., Li, X.H., Li, Q.L., 2014. When did the subduction first initiate in the southern Paleo-Asian Ocean: new constraints from a Cambrian intra-oceanic arc system in West Junggar, NW China. *Earth Planet. Sc. Lett.* 388, 222–236.
- Roser, B.P., Korsch, R.J., 1986. Determination of tectonic setting of sandstone-mudstone suites using  $\text{SiO}_2$  content and  $\text{K}_2\text{O}/\text{Na}_2\text{O}$  ratio. *J. Geol.* 94 (5), 635–650.
- Roser, B.P., Korsch, R.J., 1988. Provenance signatures of sandstone-mudstone suites determined using discriminant function analysis of major-element data. *Chem. Geol.* 67 (1–2), 119–139.
- Shia, J.G., Vajda, V., Pan, Y.H., Larsson, L., Yao, X.G., Zhang, X.L., Wang, Y.Q., Cheng, X.S., Jiang, B.Y., Deng, S.H., Chen, S.W., Peng, B., 2011. The Stratigraphy of Triassic-Jurassic boundary successions of southern margin of Junggar Basin, northwestern China. *Acta Geol. Sin. Engl.* 85, 421–436.
- Shao, L.Y., Zhang, P.F., Hilton, J., Gayer, R., Wang, Y.B., Zhao, C.Y., Luo, Z., 2003. Paleoenvironments and paleogeography of the lower and lower Middle Jurassic coal measures in the Turpan-Hami oil-prone coal basin, northwestern China. *AAPG Bull.* 87, 335–355.
- Shu, L.S., Charvet, J., Guo, L.Z., Lu, H.F., Laurent-Charvet, S., 1999. A large-scale palaeozoic dextral ductile strike-slip zone: the Aqqikkudug–Weiyea zone along the northern margin of the central Tianshan Belt, Xinjiang, NW China. *Acta Geol. Sin.* 73 (2), 148–162.

- Shu, L.S., Chen, Y.T., Lu, H.F., Charvet, J., Laurent-Charvet, S., Yin, D.H., 2000. Paleozoic accretionary terranes in Northern Tianshan, NW China. *Chinese J. Geol.* 19 (3), 193 (in Chinese with English abstract).
- Sugitani, K., Horuchi, Y., Adachi, M., Sugisaki, R., 1996. Anomalously low Al<sub>2</sub>O<sub>3</sub>/TiO<sub>2</sub> values for Archean cherts from the Pilbara Block, Western Australia—possible evidence for extensive chemical weathering on the early earth. *Precambrian Res.* 80, 49–76.
- Sun, G., Miao, Y.Y., Mosbrugger, V., Ashraf, A.R., 2010. The Upper Triassic to Middle Jurassic strata and floras of the Junggar Basin, Xinjiang, Northwest China. *Palaeobio. Palaeoenv.* 90, 203–214.
- Sun, G.Z., Liu, Y.Q., 2009. The preliminary analysis of the uplift time of Bogda Mountains, Xinjiang, Northwest China. *Acta Sedimentol. Sin.* 27, 487–493 (in Chinese with English abstract).
- Sun, M., Long, X.P., Cai, K.D., Jiang, Y.D., Wang, B.Y., Yuan, C., Zhao, G.C., Xiao, W.J., Wu, F.Y., 2009. Early Paleozoic ridge subduction in the Chinese Altai: insight from the marked change in Zircon Hf isotopic composition. *Sci. China Ser D-Earth Sci.* 52, 1345–1348.
- Sun, S., Chen, A.Q., Chen, H.D., Hou, M.C., Yang, S., Xu, S.L., Wang, F., Huang, Z.F., Ogg, J.G., 2022. Early Permian chemical weathering indices and paleoclimate transition linked to the end of the coal-forming episode, Ordos Basin, North China Craton. *Palaeogeogr. Palaeoclimatol. Palaeoecol.* 585, 110743.
- Tang, W.H., Zhang, Z.C., Li, J.F., Li, K., Chen, Y., Guo, J., 2014. Late Paleozoic to Jurassic tectonic evolution of the Bogda area (Northwest China): evidence from detrital zircon U-Pb geochronology. *Tectonophysics* 626, 144–156.
- Tao, S., Xu, Y.B., Tang, D.Z., Xu, H., Li, S., Chen, S.D., Liu, W.B., Cui, Y., Gou, M.F., 2017. Geochemistry of the Shitoumei oil shale in the Santanghu Basin, Northwest China: Implications for paleoclimate conditions, weathering, provenance and tectonic setting. *Int. J. Coal Geol.* 184, 42–56.
- Taylor, S.R., McLennan, S.M., 1985. The Continental Crust: Its Composition and Evolution, An Examination of the Geochemical Record Preserved in Sedimentary Rocks. Blackwell Scientific Publishing, Oxford, pp. 117–140.
- Taylor, S.R., McLennan, S.M., 1995. The geochemical evolution of the continental crust. *Rev. Geophys.* 33 (2), 241–265.
- Vincent, S.J., Allen, M.B., 2001. Sedimentary record of Mesozoic intracontinental deformation in the eastern Junggar Basin, northwest China: Response to orogeny at the Asian margin. In: Hendrix, M.S., Davis, G.A. (Eds.), Paleozoic and Mesozoic Tectonic Evolution of Central Asia: From Continental Assembly to Intracontinental Deformation, 194. Geological Society of America Memoir, Boulder, Colorado, pp. 341–360.
- Wali, G., Wang, B., Cluzel, D., Zhong, L.L., 2018. Carboniferous – early Permian magmatic evolution of the Bogda Range (Xinjiang, NW China): Implications for the late Paleozoic accretionary tectonics of the SW Central Asian Orogenic Belt. *J. Asian Earth Sci.* 153, 238–251.
- Wan, Y.Z., Zhou, L.F., Bai, B., Xie, Q.F., Pu, L., 2009. Provenance analysis of Shuixigou Group in southern margin of Junggar Basin. *Lithologic Reservoirs* 21, 35–41 (in Chinese).
- Wang, H.H., Wu, K.Y., Pei, Y.W., Guo, W.J., Liu, B., 2015. Evolution characteristics and physical simulation of thrust strike slip structures in Zhayier mountains. *J. Geom.* 21, 56–65 (in Chinese).
- Wang, J.B., Xu, X., 2006. Post collisional tectonic evolution and mineralization in Northern Xinjiang. *Acta Geol. Sin.* 80, 23–31 (in Chinese with English abstract).
- Wang, J.L., Wu, C.D., Li, Z., Zhu, W., Zhou, T.Q., Wu, J., Wang, J., 2018. The tectonic evolution of the Bogda region from late Carboniferous to Triassic time: evidence from detrital zircon U-Pb geochronology and sandstone petrography. *Geol. Mag.* 155, 1063–1088.
- Wang, J.R., Li, T.D., Tian, L.P., Yu, M., Wang, H.T., Zhao, Z.X., Tang, Z.L., 2010. Late Paleozoic tectono-magmatic evolution in Bogda Orogenic Belt, Xinjiang: evidence from geochemistry of volcanic rocks. *Acta Petrol. Sin.* 26, 1103–1115 (in Chinese with English abstract).
- Wang, J.W., He, Y.L., Xu, L., Xu, W.B., Wang, H.T., 2023b. Chronology and geochemistry of late Carboniferous volcanics in Bogda, Xinjiang: implications for the tectonic evolution of the Eastern Tianshan. *Front. Earth Sci.* 11, 1251107.
- Wang, J.X., Sun, P.C., Liu, Z.J., Li, Y.J., 2021. Characteristics and genesis of lacustrine laminar coal and oil shale: a case study in the Dachanggou Basin, Xinjiang, Northwest China. *Mar. Petrol. Geol.* 126, 104924.
- Wang, J.X., Sun, P.C., Bai, Y.Y., Liu, Z.J., Cheng, R.H., Li, Y.J., 2022. Carbon isotopes of n-alkanes allow for estimation of the CO<sub>2</sub> pressure in the early Jurassic - a case study from lacustrine shale and cannel boghead in the Dachanggou Basin, Xinjiang, Northwest China. *Palaeogeogr. Palaeoclimatol. Palaeoecol.* 607, 111252.
- Wang, Q., Zhao, G.C., Han, Y.G., Yao, J.L., 2020. Detrital zircon constraints on late Paleozoic tectonism of the Bogda region (NW China) in the southern Central Asian Orogenic Belt. *Geosci. Front.* 11 (5), 1533–1548.
- Wang, S.Z., Yu, H.Z., Li, B.S., Han, J.Q., Zhap, C., Guo, Y.Y., Liu, J.Y., Su, C., Chang, X., Wu, T., Huang, H.Q., 2025. Provenance and tectonic controls in eastern Junggar: Insights from petrography and REE geochemistry. *Molecules* 30, 3399.
- Wang, X.R., Cheng, W., Xu, R.D., 2023a. Adsorption of rare earth elements on organic matter in coal. *J. Rare Earth* 41, 1108–1115.
- Wang, X.W., 2016. The Late-Paleozoic Volcanic Rocks in the Eastern Bogda of Eastern Tianshan: Petrology, Geochemistry and Structure Property. Dissertation for Doctoral Degree. School of Earth Science and Resources, Chang'an University, Shaanxi (in Chinese with English abstract).
- Wang, Z.X., Li, T., Zhang, J., Liu, Y.Q., Ma, Z.J., 2008. The uplifting process of the Bogda Mountain during the Cenozoic and its tectonic implication. *Sci. China Ser D-Earth Sci.* 51, 579–593.
- Wartes, M.A., Carroll, A.R., Greene, T.J., 2002. Permian sedimentary record of the Turpan–Hami basin and adjacent regions, northwest China: constraints on post-malgamation tectonic evolution. *Geol. Soc. Am. Bull.* 114, 131–152.
- Wiedenbeck, M., Alle, P., Corfu, F., Griffin, W.L., Meier, M., Oberli, F., Quadri, A.V., Roddick, J.C., Spiegel, W., 1995. Three natural zircon standards for U-Th-Pb, Lu-Hf, trace element and REE analyses. *Geostand. Newsl.* 19 (1), 1–23.
- Windley, B.F., Alexeev, D., Xiao, W.J., Kröner, A., Badarch, G., 2007. Tectonic models for accretion of the Central Asian orogenic belt. *J. Geol. Soc. Lond.* 164, 31–47.
- Wong, K., Sun, M., Zhao, G.C., Yuan, C., Xiao, W.J., 2010. Geochemical and geochronological studies of the Alegedai Ophiolitic complex and its implication for the evolution of the Chinese Altai. *Gondw. Res.* 18 (2–3), 438–454.
- Xiao, D., Zhao, X.Y., Liao, Q.A., Zhao, L., 2013. Early Palaeozoic arc-related gabbro-diorite suite in East Junggar, southern Central Asian Orogenic Belt: petrogenesis and tectonic implications. *Int. Feol. Rev.* 48, 1050–1068.
- Xiao, W.J., Santosh, M., 2014. The western Central Asian Orogenic Belt: a window to accretionary orogenesis and continental growth. *Gondw. Res.* 25 (4), 1429–1444.
- Xiao, W.J., Zhang, L.C., Qin, K.Z., Sun, S., Li, J.L., 2004. Paleozoic accretionary and collisional tectonics of the Eastern Tianshan (China): Implications for the continental growth of Central Asia. *Am. J. Sci.* 304, 370–395.
- Xiao, W.J., Han, C.M., Yuan, C., Sun, M., Lin, S.F., Chen, H.L., Li, Z.L., Li, J.L., Sun, S., 2008. Middle Cambrian to Permian subduction-related accretionary orogenesis of Northern Xinjiang, NW China: Implications for the tectonic evolution of Central Asia. *J. Asian Earth Sci.* 32 (2–4), 102–117.
- Xiao, W.J., Windley, B.F., Yuan, C., Sun, M., Han, C.M., Lin, S.F., Chen, H.L., Yan, Q.R., Liu, D.Y., Qin, K.Z., Li, J.L., Sun, S., 2009. Paleozoic multiple subduction-accretion processes of the southern Altaiids. *Am. J. Sci.* 309, 221–270.
- Xiao, W.J., Huang, B.C., Han, C.M., Sun, S., Li, J.L., 2010. A review of the western part of the Altaiids: a key to understanding the architecture of accretionary orogens. *Gondw. Res.* 18, 253–273.
- Xie, W., Xu, Y.G., Chen, Y.B., Luo, Z.Y., Hong, L.B., Ma, L., Liu, H.Q., 2016. High-alumina basalts from the Bogda mountains suggest an arc setting for Chinese northern Tianshan during the late Carboniferous. *Lithos* 256–257, 165–181.
- Xu, J., Stockli, D.F., Snedden, J.W., 2017. Enhanced provenance interpretation using combined U-Pb and (U-Th)/He double dating of detrital zircon grains from lower Miocene strata, proximal Gulf of Mexico Basin, North America. *Earth Planet. Sci. Lett.* 475, 44–57.
- Xu, Q.Q., Zhao, L., Niu, B.G., Zheng, R.G., Yang, Y.Q., Liu, J.H., 2020. Early Paleozoic arc magmatism in the Kalamaili orogenic belt, Northern Xinjiang, NW China: Implications for the tectonic evolution of the East Junggar terrane. *J. Asian Earth Sci.* 194 (1), 104072.
- Xu, X.W., Jiang, N., Li, X.H., Wu, C., Qu, X., Zhou, G., Dong, L.H., 2015. Spatial-temporal framework for the closure of the Junggar Ocean in central Asia: New SIMS zircon U-Pb ages of the ophiolitic mélange and collisional igneous rocks in the Zhifang area, East Junggar. *J. Asian Earth Sci.* 111, 470–491.
- Xu, X.Y., Li, R.S., Chen, J.L., Ma, Z.P., Li, Z.P., Wang, H.L., Bai, J.K., Tang, Z., 2014. New constrains on the Paleozoic tectonic evolution of the northern Xinjiang area. *Acta Petrol. Sin.* 30 (6), 1521–1534 (in Chinese with English abstract).
- Yan, D.T., Chen, D.Z., Wang, Q.C., Wang, J.G., 2010. Large-scale climate fluctuations in the latest Ordovician on the Yangtze block, South China. *Geology* 38, 599–602.
- Yang, G.X., Li, Y.J., Wu, H.E., Zhong, X., Yang, B.K., Yan, C.X., 2011. Geochronological and geochemical constrains on petrogenesis of the Huangyangshan A-type granite from the East Junggar, Xinjiang, NW China. *J. Asian Earth Sci.* 40 (3), 722–736.
- Yang, Y.T., Song, C.C., He, S., 2015. Jurassic tectonostratigraphic evolution of the Junggar basin, NW China: a record of Mesozoic intraplate deformation in Central Asia. *Tectonics* 34, 86–115.
- Yang, Y.X., Zhang, J.F., Zhang, J.H., Gao, Y.J., Zhou, X.G., Sun, X.C., Wen, L., Miao, M.Q., 2022. Sedimentary characteristics and main controlling factors of the Middle-Upper Permian and Middle-Upper Triassic around Bogda Mountain in Xinjiang, NW China. *Petrol. Explor. Dev.* 49, 770–784.
- Yarmolyuk, V.V., Kovalenko, V.I., Salnikova, E.B., Kovach, V.P., Kozlovsky, A.M., Kotov, A.B., Lebedev, V.I., 2008. Geochronology of igneous rocks and formation of the late Paleozoic south Mongolian active margin of the Siberian continent. *Stratigr. Geo. Correl.* 16, 162–181.
- Yuan, C., Sun, M., Xiao, W.J., Li, X.H., Chen, H.L., Lin, S.F., Xia, X.P., Long, X.P., 2007. Accretionary orogenesis of the Chinese Altai: insights from Paleozoic granitoids. *Chem. Geol.* 242, 22–39.
- Zhang, C.H., Liu, D.B., Zhang, C.L., Wang, Z.Q., Yu, Q.X., 2005b. Stratigraphic constraints on the initial uplift age of Bogda Shan, Xinjiang, north-West China. *Earth Sci. Front.* 12, 294–302 (in Chinese with English abstract).
- Zhang, H., Kuang, H.W., Liu, Y.Q., Peng, N., 2013a. The sedimentary differences of the Middle Jurassic Xishanyao Formation between Santanghu area and Turpan-Hami area and their constraints on the uplifting of the Bogda Mountain. *Geol. Bull. China* 32, 443–455 (in Chinese with English abstract).
- Zhang, L., He, D.F., Yi, Z.J., Li, D., 2020. Tectonic relationship between the Kelameili range and the Dajing depression: Insights into the Carboniferous tectonic-sedimentary framework. *Petrol. Explor. Dev.* 47, 30–45.
- Zhang, Y.Y., Pe-Piper, G., Pipier, D.J.W., Guo, Z.J., 2013b. Early Carboniferous collision of the Kalamaili orogenic belt, North Xinjiang, and its implications: evidence from molasse deposits. *Geol. Soc. Am. Bull.* 125 (5–6), 932–944.
- Zhang, Y.Y., Guo, Z.J., Pe-Piper, G., Piper, D.J.W., 2015. Geochemistry and petrogenesis of early Carboniferous volcanic rocks in East Junggar, North Xinjiang: Implications for post-collisional magmatism and geodynamic process. *Gondw. Res.* 28 (4), 1466–1481.
- Zhang, Y.Y., Yuan, C., Long, X.P., Sun, M., Huang, Z.Y., Du, L., Wang, X.Y., 2017. Carboniferous bimodal volcanic rocks in the Eastern Tianshan, NW China: evidence for arc rifting. *Gondw. Res.* 43, 92–106.

- Zhang, Y.Y., Tian, J.J., Feng, S., Yang, F., Lu, X.Y., 2018. The occurrence modes and geologic origins of arsenic in coal from Santanghu Coalfield, Xinjiang. *J. Geochem. Explor.* 186, 225–234.
- Zhang, Z.Z., Gu, L.X., Wu, C.Z., Li, W.Q., Xi, A.H., Wang, S., 2005a. Zircon SHRIMP dating for the Weiya Pluton, eastern Tianshan: its geological implications. *Acta Geol. Sin.* 79, 481–490.
- Zhao, L., Yang, Y.Q., Zheng, R.G., Xu, Q.Q., 2024. An evolving tectonic environment of early to Middle Permian granitic plutons in the Barkol area, East Junggar: insights from integrated zircon U-Pb ages, geochemistry, and Nd-Sr-Hf isotopes. *Int. Geol. Rev.* 66 (8), 1465–1478.
- Zhao, L.S., Liu, B., Wen, Z.G., Hu, Z.W., 2025. Astronomical forcing of lake-level changes along the low-latitude Asian continental margin and the global sea level responses during the early-middle Eocene. *J. Asian Earth Sci.* 280, 106470.
- Zhou, J.B., Zhuang, X.G., Alastuey, A., Querol, X., Li, J.H., 2010. Geochemistry and mineralogy of coal in the recently explored Zhundong large coal field in the Junggar basin, Xinjiang province, China. *Int. J. Coal Geol.* 82 (1–2), 51–67.
- Zhou, T.Q., Wu, C.D., Yuan, B., Shi, Z.K., Wang, J.L., Zhu, W., Zhou, Y.X., Jiang, X., Zhao, J.Y., Wang, J., Ma, J., 2019. New insights into multiple provenances evolution of the Jurassic from heavy minerals characteristics in southern Junggar Basin, NW China. *Petrol. Explor. Dev.* 46, 67–81.
- Zhou, Y., Liu, Z.L., Mänd, K., Li, F.J., Peng, N., Kuang, H.W., Liu, Y.Q., Liu, Y.X., Zhang, M.H., 2022. Geochemical characteristics of Jurassic sandstones on the southern margin of the Junggar Basin: Constraints on provenance and sandstone-type uranium mineralization. *Ore Geol. Rev.* 146, 104922.
- Zong, K.Q., Klemd, R., Yuan, Y., He, Z.Y., Guo, J.L., Shi, X.L., Liu, Y.S., Hu, Z.C., Zhang, Z.M., 2017. The assembly of Rodinia: the correlation of early Neoproterozoic (ca. 900Ma) high-grade metamorphism and continental arc formation in the southern Beishan Orogen, southern Central Asian Orogenic Belt (CAOB). *Precambrian Res.* 290, 32–48.